Nordic Volcanological Institute 8103

THE ERUPTION OF THE THORSMÖRK IGNIMBRITE, SOUTH ICELAND

THE STRUCTURE OF THE MAGMA CHAMBER DEDUCED FROM THE ERUPTION PRODUCTS

by

Karl A. Jørgensen

1980

ABSTRACT

The Thorsmörk ignimbrite, S. Iceland, is one of the largest eruptive bodies recorded from Iceland. Studies of the tephra shows that the eruption started comparatively quietly but gained in violence with time, evidenced by changes in the vesiculation pattern of the acid glass. The minerals, anorthoclase, ferro-hedenbergite, ilmenite, magnetite and fayalite record changes in magmatic temperatures and oxygen fugacities with both time and stratigraphic height. Geothermometry indicates magmatic temperatures from 900 to 960°C around the FMQ buffer in the first erupted magma, but intrusion of basic magma into the acid magma chamber raised the temperature of the remaining magma to approximately 1040°C, and produced a variety of hybrid compositions. Environmental considerations indi-cate that the magma chamber was situated at the depth of 3 to km. Different glass compositions indicate an ori-gin of the main rhyolitic body through fractional crystal-lization of a rhyodacitic parent.

INTRODUCTION

The Thorsmörk ignimbrite (Thorarinsson, 1969) is a late Pleistocene pyroclastic complex flow, which is exposed in the valley area of Thorsmörk in southern Iceland (Fig. 1). The ignimbrite originated within the caldera region of the Tindfjallajökull silicic center, which is one of a group of at least 5 closely spaced silicic centers in the southern part of the Eastern Volcanic Zone of Iceland, an area characterized by a heterogeneous tectonic stress pattern (Sæmundsson, 1978). The five silicic centers show contrasting geochemical trends from the almost calc-alkaline Hekla center to the slightly peralkaline Torfajökull center (Imsland, 1978). The regional volcanism is characterized by the production of high Fe-Ti tholeiites transitional to alkaline basalts (Jakobsson, 1972; Imsland, 1978). The Tindfjallajökull silicic center is dominated by slightly alkaline basalts and minor intermediate rocks with abundant subalkaline to slightly peralkaline rhyolites (Larsen & Jørgensen, in prep.). The Thorsmörk ignimbrite is one of the largest acid eruptive bodies recorded from mid-oceanic islands. It has not been dated radiometrically, but belongs stratigraphically to the penultimate interglacial stage of the area, indicating an age of approximately 200.000 years. The event postdates the main caldera formation of the Tindfjallajökull silicic center by a significant amount of time (several thousands of years).

Following a preliminary study (Jørgensen, in press), this paper presents the results of a more detailed petrological study of the Thorsmörk ignimbrite designed to throw light on the eruption history and the pre-eruption conditions prevailing in the magma chamber.

PREVIOUS INVESTIGATIONS

The Thorsmörk ignimbrite was originally described and its main features outlined by Thorarinsson (1969) and Jørgensen (in press). A few petrologic data have been published by Sigurdsson (1970) and Wetzel et al. (1978).

The ignimbrite outcrops over an area of 80 km^2 and is extensively covered with later volcanics. It averages 20 m in thickness but in places it attains a thickness of 200 m. It originally buried a landscape with features very similar to those of the present landscape in the area. Later erosion has mainly removed the soft, unwelded parts of the ignimbrite.

A careful calculation gives an original estimated volume of the ignimbrite of 8 km^3

In the field the ignimbrite is readily divided into four parts,

top
4) white to buff, unwelded, 0-70 m
3) grey, welded and devitrified, 0-75 m
2) black, welded vitrophyre, 0-15 m
1) light, unwelded tephra, 0-1 m
base.

This division is the result of the post emplacement processes of compaction and devitrification. The welded and devitrified parts wedge out towards the distal parts of the ignimbrite.

In the ignimbrite it is possible to distinguish a number of flow-units (at least 10), on the basis of topographic breaks, internal stratification, normal grading of lithics, and reverse grading of pumice clasts as well as mineralogical changes.

Lithic-rich bands occur with increasing frequency up through the ignimbrite culminating in a 15 m thick deposit consisting of 75% by weight of lithic fragments, close to the top of the ignimbrite. Above the xenolithic unit only two or three flow-units occur, and these have thin, fine-

grained sediments of supposed niveo-eolian (Cailleux, 1978) origin intercalated between the flow-units.

The unwelded part of the ignimbrite has an average modal composition as follows:

Pumice	13%
Crystals	10%
Mafic glass	3%
Lithics	10%
Matrix	64%

The variations are, however, very large as seen in Table I.

The present study is mainly concerned with the acid pumice and crystals, but both the mafic glass and the lithics will be described briefly as they have important bearings on the origins of the ignimbrite.

Methods of the study

To investigate the composition of the glasses and their associated phenocrysts a number of vitric samples were selected to cover both the stratigraphic range as well as the range of vitric types observed.

To obtain compositions of glasses and phenocrysts in known petrographic settings most of the analysed samples were thin sections of whole-rock rather than of mineral separates. Point counting of heavy mineral separates were, however, used to determine the relative abundance of the different heavy phases.

The locations of the analysed samples are shown in Fig. 1, and the general features of the samples given in Table I.

Analytical methods

The phenocrysts and glasses were analysed with an ARL SEMQ microprobe using on-line corrections of Bence & Albee (1968) and various natural standards. The operating conditions were: Accel. pot. 15 kV, sample current 25 nA for mafic minerals and 10 nA for feldspars and glasses. Counting times 20 sec. peak and 4 sec. background on each side. During glass-analysis samples were moved continuously to avoid alkali loss. For very small areas of glass a procedure with only 10 sec. peak and 2 sec. background was used with reasonable success.

THE VESICULATION OF THE MAGMAS AND THE ERUPTION HISTORY

During examination of the samples used for mineralogical studies an apparently systematic change in the vesiculation pattern of the glass was observed. These observations have been quantified, and the main results are presented in Table II.

The acid glass (refractive index <1.51, colourless to greyish) can be divided into a number of types. The most conspicuous are pumice clasts with sizes up to 40 cm in diameter. They are generally strongly vesiculated (Table II) and have ovoid to pipelike vesicles, which have often been folded. In the lower part of the ignimbrite, the vesicles are regular with smooth walls, while in the upper part, vesicles often are irregular and have rough surfaces, due to disruption of already formed vesicles by new generations of vesicles (multiple vesiculation). The proportion of pipe-vesicles declines upwards in the ignimbrite (Table II, 30474 is abnormal). Two types of vesicles are found developed around phenocrysts in the pumice clasts: (1) large and equant vesicles with diameters of 1-2 mm, which are found irregularly distributed around the phenocryst, (2) a regular system of elongate vesicles which radiate out from the phenocryst (the radial vesicles of Heiken & Eichelberger (1980)). In some cases Fig. 2, these radial vesicles can be seen to distort the surrounding pipe-vesicles.

The shards range in size from 100 to 1000 µm (Table II) and are generally Y-shaped, though equant shards predominate in the lowermost part of the ignimbrite, Fig. 4, and star-shaped shards in the uppermost part, Fig. 3. The size and shape of the shards indicate that they originated through the rupture of spherical to ovoid, large thick-walled vesicles of a fairly uniform size range, contrary to the vesicles in the pumices, where walls between large vesicles always contain smaller vesicles. The glass shards generally have a well developed secondary hydration rind with a thickness of 10 µm.

In the lowermost part of the ignimbrite occasional bits of little vesiculated glass are found (Table II), these

grade continuously into more vesiculated clasts, Fig. 4.

Normally the acid glass is colourless and transparent, but occasionally, in the lower part of the ignimbrite, some clasts with a texture and colour distinctly different from those described above occur. These clasts consist of grey to greyish-brown glass with short pipe-vesicles, often with spherical extensions giving a very variable wall thickness ranging from 20 to 100 µm, often within the same wall between two vesicles. The glass often shows flow lineation. Chemical analyses (see later) show that these glasses are lower in silica (approx. 70% SiO_2) than the usual acid glass (approx. 74% SiO_2). The chemical investigation also revealed the existence of a high silica glass (approx. 76% SiO_2) in the lowermost part of the ignimbrite, but this type is indistinguishable from the normal pumices and has not been found as shards.

In the lower part of the ignimbrite are found fresh angular fragments of a non-vesiculated glassy, flow-lineated rock with abundant microlites of plagioclase and pyroxene. Chemical analyses (Table IV) shows it to be very similar to the lower silica acid glass described above. The freshness of the fragments and absence of more crystalline or spheroidal types strongly suggests a very recent age with respect to the ignimbritic eruption.

The mafic glasses (refractive index between 1.52 and 1.60, colour brownish to brown to opaque) present a variety of textures and compositions indicative of multistage mixing, represented by different types of banded pumices, between a normal transitional basalt and one or more silicic end-members, resulting in the formation of various glasses ranging in composition from 46 to 71% SiO_2, with associated microcrystal and xenocrystal phases as well as a wealth of different vesiculation textures which presently are being investigated.

The basic end-member glasses show a range of textures from strongly vesiculated types reminescent of acid pumices over more equant types with large regular vesicles similar

to types commonly found in strombolian deposits as described by Walker & Croasdale (1972), to small perfect spheres up to .05 mm in size very similar to the spheres from Kilauea Iki described by Heiken (1972) as characteristic of Hawaiian type fountaining.

DISCUSSION

Vesiculation of magma has achieved much attention in recent years (McBirney, 1973; Bennett, 1974; Sparks, 1978; Heiken, 1972; Heiken & Eichelberger, 1980). The Thorsmörk ignimbrite shows features which are compatible with the conclusions of most of these authors.

The low degree of vesiculation observed in the initial eruption products, as well as the equant shards, is reminescent of the tephra textures observed in phreatomagmatic eruption products (Heiken, 1972), and could be interpreted as initiated by pockets of trapped meteoric water in the way proposed by McBirney (1973). After this initiation the nucleation of vesicles would proceed aided by the thermal gradient established by the intruding basic magma (see later), and possibly by the formation of the downwards-migrating expansion waves proposed by Bennett (1974). These would regularly disrupt the magma surface and vesiculation process, leading to the formation of the multistage vesiculated pumices described.

It is even possible that the eruption started with an effusive phase, as the fresh, low-silica rhyolite fragments found in the lower part of the ignimbrite, may have been torn from an initially extruded coulee or dome.

With time, vesiculation increased, partly helped by nucleation around the abundant phenocrysts, leading to the formation of the large equant vesicles. Evidence of radial vesiculation is only found in the pumices, indicating that this process first became active after disruption of the magma surface. This probably indicates the importance of

the adiabatic cooling of the magma relative to the phenocrysts, leading to the pool-boiling proposed by Heiken & Eichelberger (1980), the force of which is evidenced by the disruption of the pipe-vesicles shown in Fig. 2.

The increasing vesiculation led to higher excess pressure in the magma-chamber, causing more violent outbursts as evidenced by the larger abrasion index (Meyer, 1972) (Table II) and the increasing frequency of lithic horizons up through the ignimbrite. The higher excess pressure may also be a function of blocking of the vent by collapsing wall rock during periods of quiescence, thus explaining the increasing time gaps between the pyroclastic flow-units evidenced by the intercalated sedimentary deposits in the uppermost part of the ignimbrite. These deposits do, however, first occur after the cataclysmic event that produced the 15 m thick xenolith-rich unit, so probably the last explanation is only valid after this event.

The eruptive sequence delineated above has been summarized in Table III.

That periods of more quiet eruptions did occur between the general pattern of increasing explosivity is evidenced by sample 30474, which has an abrasion index similar to that of the earliest flow-units. It is probably also significant that this sample does not contain any hybrid compositions (Table I).

Sparks & Wilson (1976) divide ignimbrites into two categories: (1) those containing an initial plinian deposit, which are likely to have developed through gravitative collapse of the eruption column, and (2) those which do not possess a plinian deposit, which either did not have a sufficient gas content or a too wide vent radius for convective thrusts to occur. The last situation is likely to occur if the explosive phase started with a phreatomagmatic event. The lack of convective thrusts in this case is further substantiated by the groundmass crystallization which took place under so reduced conditions (see later),

that it is unlikely that any atmospheric air of importance had had the opportunity to mix with the pyroclastic material.

SHAPE OF THE ERUPTIVE CONDUIT

The simultaneous occurrence of glasses of highly different compositions poses the question of how these glasses were erupted.

The common occurrence of banded clasts shows that the magmas mingled prior to eruption, most probably in the eruptive conduit. However, some system seems to exist with respect to the banded clasts. Thus the banded clasts com-posed of low and normalacid glass are mostly found in the lowermost part of the ignimbrite, while the mafic/silicic clasts, though ubiquitous in the ignimbrite, are much more common in the upper part than in the lower part. The occur-rence of unmixed basic scoriae and glass spheres further suggests very low explosivity in some parts of the conduit.

The most probable shape of the conduit is thus a dyke or fissure of the classic Icelandic type (Guppi & Hawkes, 1925), with a thin basaltic margin and a thick acid core, which becomes purely basaltic in the distal parts of the fissure, and probably developes into a row of craters each producing material of individual character, a well known feature for several large, Icelandic postglacial eruptions, such as the Domadalshraun eruption (Sæmundsson, 1972; pers. observation).

PETROCHEMISTRY OF THE ACID GLASSES

Approximately 95% of the acid glass present is a comenditic rhyolite with a narrow compositional range, apparently unrelated to stratigraphy, Table IV, Fig. 5. There is a tendency for pumices to show a larger scatter of compositions than do the shards but this is the result of secondary hydration of the thin-walled pumices.

The high silica compositions have higher agpaitic indexes than the average rhyolite, and also significantly lower Na_2O/total alkali ratios. The trace element pattern is consistent with the rising agpaitic index showing a rise in Ba, Zr, La and Nb and a fall in Sr, V and Y.

The low silica compositions (and the microcrystalline fragments) have lower agpaitic index, and are more similar to rhyodacites from tholeiitic centres (Carmichael, 1964; Grönvold, 1972).

The peralkaline rhyolites are clearly oceanic comendites after the classification of Bailey & Macdonald (1970) and rather similar to the comendites from Easter Island (Bailey & Macdonald, op.cit.; Baker et al., 1974), Fig. 6.

THE PHENOCRYSTS

The ignimbrite contains an average of 12% by weight of phenocrysts coexisting with the acid glass, distributed as follows (in weight %):

Feldspar	10.8 %	
Pyroxene	1.0 %	
Olivine	.005 %	(up to .3%)
Ore	.1 %	
Zircon	.02 %	
Chevkinite	.005 %	
Apatite	.005 %	

(These figures are weighted averages deduced from point counting of heavy and light mineral/glass separates, except for apatite which was estimated by comparison with chevkinite in thin sections. Representative densities were adopted from Tröger (1971)).

The phenocrysts mainly occur as discrete crystals (or as abraded fragments of such) or as inclusions in other minerals, but small crystal clusters are common, and in the lowermost part of the ignimbrite large loose aggregates are characteristic.

The minerals display small, but significant changes in texture and composition which record a story of fractional crystallization under comparatively stable conditions suddenly interrupted by a change in the physical conditions immediately prior to the eruption.

The feldspars

The feldspars occur as three different types, Table V.

The inclusions in type 1 and 2 feldspars are especially pyroxene, often with a vermicular habit. Ore minerals, especially magnetite are common as inclusions, often as small clusters of octahedra. Fayalite is only rarely found as inclusions, even where the mineral is most abundant as discrete phenocrysts, and then only intergrown with the rim of the feldspar. Minute needles of apatite and chevkinite are common as inclusions, mostly in the rims of the type 1 phenocrysts. The apatite is often associated with inclusions of ferromagnesian phases, preferably magnetite. Glass inclusions, occasionally with gas vesicles, occur mainly in the type 2 phenocrysts, or in the outer part of type 1 phenocrysts.

Most of the feldspars are optically slightly normally zoned, occasionally with a thin, distinct core and/or a thin rim, but type 1 feldspars may show oscillatory zoning and resorption phenomena, and patchy zoning is common in this type. Oscillatory zoning is restricted to the lower 50 m of the ignimbrite, while resorption and patchy zoning are found throughout the ignimbrite. Approximately 5% of the feldspars present are oscillatory zoned or resorbed, while 10% are patchy zoned.

In many feldspars glass inclusions situated close to the rim have broken open immediately prior to eruption due to the fracturing of the feldspar. Similarly totally broken phenocrysts, although with the fragments in their approximate original positions, may be found in the pumices.

Both phenomena are evidence for a drastic shock effect, probably an expansion wave followed by a fall in the confining pressure, as described under vesiculation (above).

Chemically the feldspars are anorthoclases, Tables V and VI, Fig. 7, ranging in composition from $An_{10}Ab_{81}Or_9$ in the cores of the largest type 1 feldspars to $An_{1.6}Ab_{78.3}Or_{20.1}$ in type 3 microcrysts. It is an overall trend that the feldspars show a steady decrease in An from core to rim, except for feldspars with Or<18, where An<2. Oscillatory zoning as well as resorption is a function of varying Ab:Or ratios, Fig. 7, and not related to fluctuations in the An:Ab ratios. There is a tendency for the feldspars from one of the lowermost samples (19337) to lie on the sodic side of the general trend, Fig. 7, while feldspars from the uppermost sample (22042) lie on the potassic side.

Of the minor elements only Fe and Ba were detected, while both Mg and Sr were below detection limit. Both FeO^t and BaO occur with average amounts of .28% by weight. Ba shows no consistent variations within the range observed, but there seems to be a minor increase in Fe from core to rim. An analysis of the Si/Al(+Fe) relationship, Fig. 8, seems to show that the relationship Si+Al=16 (in formula units) in general is fulfilled, thus suggesting that the iron is mainly present as Fe^{2+}, except in the most calcic cores, the microcrysts and the least sodic (22042) feldspars, where the iron mainly seems to substitute for Al.

The pyroxenes

As is the case with the feldspars a triple division can be made for the pyroxenes, Table VII, though the transitions are more gradational than for the feldspars.

In general the pyroxenes are grass-green to yellow-green, subhedral to euhedral, homogeneous crystals, except in aggregates with feldspar where they have crystallized after the feldspar, and attain a granular or vermicular habit.

The inclusions are predominantly euhedral ilmenite and magnetite as well as small euhedral zircons, stubby prisms of chevkinite, small needles of apatite, rare rounded blebs of pyrrhotite and occasionally large elongate glass inclusions, mainly occurring in the center orientated after the c-axis.

Twinning is very rare but has been observed both on (100) and (010) (U-stage determinations).

Chemically the pyroxenes are ferro-hedenbergites ranging from $Wo_{43.0}En_{4.5}Fs_{48.6}Ac_{3.8}$ to $Wo_{43.3}En_{.8}Fs_{51.0}Ac_{4.9}$ (Tables VII and VIII and Fig. 9) with the most magnesian compositions representing the largest type 1 cores. All pyroxenes show a ubiquitous, weak normal zoning.

There is an overall tendency towards a decrease in calcium with a decreasing magnesium content, Fig. 9, and a minor decrease in alumina and increase in sodium, Figs. 10 and 11. The low contents of alumina makes it difficult to distribute it between Al^{IV} and Al^{VI}, but in general the relationship Si+Al=2 is unsatisfied to satisfied, suggesting that most of the alumina is Al^{IV}. If this is true, then it seems as though there is an overall trend in Ti/Al from 1:2 to 1:1 relationship from cores to rims of type 1 pyroxenes, Fig. 12, indicating stabilization of a NAT-component (Rønsbo et al., 1977), at the expense of the Ca-Ti-Tschermak´s component.

In rare cases pyroxene phenocrysts are found with a distinct pale yellow core of calcic ferro-augite ($Wo_{44.8}En_{26.0}Fs_{29.2}$) mantled by a thick, deep green rim, of ferro-hedenbergitic to sodic ferro-hedenbergitic composition (Table VIII, Fig. 13). The pale core contains abundant apatite inclusions.

In a few cases quenched clots of acid material have been observed. These contain grass-green, needle shaped pyroxenes high in alumina and manganese and low in calcium and sodium (Table VIII, and Figs. 11 and 13). They are associated with acicular magnetite and tabular feldspar.

In composite pumices, consisting of "normal" 74% SiO_2 glass and "low" silicic 70% SiO_2 glass, microcrysts of

grass-green pyroxene, high in alumina and titanium (Table VIII, Figs. 11 and 13) have crystallized in the low silica glass along with microcrysts of ilmenite and feldspar.

The olivine

The olivine occurs as honey-coloured, equant crystals approximately .5 mm in size with rare elongated individuals up to 1 mm in length.

The olivine is generally crowded with inclusions of euhedral Fe-Ti oxides, chevkinite, apatite and glass-tubuli, and often occurs in small aggregates with pyroxenes, ore and feldspar.

The olivine is often slightly altered and oxidized at the rim. Commonly only an empty mould in the matrix is found, occasionally with some Fe-Ti oxide and mineral inclusions remaining.

Chemically the olivine is an almost pure fayalite with a uniform composition of $Fo_{.5}Fa_{94.7}Tp_{4.2}Ln_{.7}$ (max. range $Fo_{.5-.4}$), Table IX, Fig. 9.

The lower parts of the ignimbrite contain up to 3% by weight of olivine, while the upper parts contain less than .01% by weight. The decrease is sudden from around .25% to .05% and occurs at a flow unit boundary at the 75 m level in the ignimbrite.

The ore minerals

The ore minerals present are ilmenite, magnetite and minor pyrrhotite. Ilmenite is the dominant phase, and occurs both as discrete, commonly large crystals, as inclusions and in aggregates with pyroxene. The crystals are on the average .2 mm in size, but occasionally up to 1 mm. In general the crystals are euhedral, displaying rhombohedral shapes, but some inclusions, especially in

feldspars, are rounded. Some of the larger discrete crystals are skeletal or have glass inclusions. In general the grains are homogeneous and exsolution phenomena rare. Some of the discrete grains have a slightly oxidized rim, probably due to post-emplacement reactions.

Magnetite occurs mainly as inclusions, predominantly in feldspar but occasionally in pyroxene and fayalite. It most often occurs as euhedral octahedral, but rounded grains are not uncommon. The size range is between .05 and .1 mm. In the upper part of the ignimbrite rare discrete crystals occur. In the lower part of the ignimbrite oxyexsolution (Buddington & Lindsley, 1964) of ilmenite lamellae after (111) are occasionally found, with the rounded grains showing the strongest oxyexsolution.

The magnetite:ilmenite ratio varies from 1:5 in the lower part of the ignimbrite to 1:1 in the uppermost part of the ignimbrite (22042). In this sample (22042) some ilmenites show exsolution of haematite lamellae, while the magnetites are homogeneous, but have a spotted appearance in reflected light.

The ilmenite and magnetite are comparatively pure ilmenite and titanomagnetite, Table X, which when plotted into the triangular $R^{2+}O$, TiO_2-$R^{2+}O$-$R^{3+}{}_2O_3$ diagram of Carmichael (1967), Figl 14, coincides with his olivine-bearing Icelandic rhyolites with tie lines parallel to his. The content of minor elements is low and totally dominated by MnO causing the minerals to plot almost on the MnO-Al_2O_3 side of Carmichael´s (op.cit.) triangular minor element plot, Fig. 15, with a very narrow range. There is a tendency for the magnetites from the lowermost (19337) and the uppermost (22042) samples to contain more of the Usp-molecule than the rest of the ignimbrite. A magnetite in a glass inclusion in a zoned pyroxene has the highest Usp-content of all the analysed magnetites, Table X.

Some ilmenites contain unusually high amounts of CaO and other trace elements and probably have a xenocrystic origin, Table X.

The pyrrhotite occurs as rare, tiny (less than 0.2 mm) globules in the oxides and in very rare cases in the pyroxenes.

Zircon

Zircon occurs as transparent, colourless, euhedral crystals up to .5 mm in length, and generally with well developed prisms and bipyramids. It commonly contains abundant inclusions of magnetite, glass tubuli, apatite prisms and very rarely chevkinite. The zircon occurs mostly as discrete crystals or in clusters with Fe-Ti oxides ± pyroxene. It is somewhat more abundant in the lower part of the ignimbrite than in the upper part.

Partial chemical analyses, Table IX, indicates an unremarkable composition.

Chevkinite

Chevkinite, a monoclinic REE iron titanosilicate, occurs both as rare, discrete, stubby prismatic crystals up to .2 mm long, and in a few cases as slender, pencil-like crystals up to .3 mm long, as well as inclusion in other silicic phases, where the stubby type seems to prefer the pyroxenes, while the slender type is most common in the fayalites and feldspars. It is generally well developed with occasional simple twins on (001). The colour ranges from redbrown in the α direction to opaque in the β and γ directions (yellow-brown to blue-green in crystals less than 10 µm thick). Some larger grains contain inclusions of apatite and occasionally an earlier generation of small chevkinite crystals. It seems to be more abundant in the lower part of the ignimbrite (up to 25 grains per thin section) than in the upper part (up to 7 grains per thin section).

A partial chemical analysis, Table IX, shows that it is very similar to other analyses of the mineral (Jaffe et al., 1956; Segalstad & Larsen, 1978) though low in alumina and magnesium and high in titanium and iron.

Apatite

Apatite occurs as minute (length max. .1 mm, width max. .015 mm) euhedral, hexagonal prisms, predominantly found as inclusions in all the other phases, but occasionally also as discrete crystals. It is rather common in the rims of the feldspars, but absent in the cores of the large type 1 feldspars. It is most abundant as inclusion in the fayalite and zircon, least in the pyroxene. Its composition is unremarkable, Table IX.

THE GROUNDMASS PHASES AND THEIR SIGNIFICANCE

Jørgensen (in press) describes the progressive crystallization in the welded part of the ignimbrite, and divides it into 6 stages from stage (1) unaltered glass, through increasing degrees of crystallization in the matrix until stage (6) where alkali-feldspar, tridymite and mafic minerals crystallize in gas cavities developed in the fused glass. Generally this most extreme development has been obscured by alteration by late stage hydrothermal fluids percolating through the vesicle system, but occasionally relict areas have been preserved. In general the assemblage found consists of tridymite, alkali-feldspar, arfvedsonite and acicular ore, probably ilmenite. However, the sample 19337, which consists of fused glass with the most peralkaline composition found in the ignimbrite, has a crystallized interior showing a different assemblage. The crystalline core can be divided into two parts. An outer part which is spherulitic with relatively few gas cavities and contains well developed fayalites and bundles of aenigmatite crystals.

The feldspar in this part is anorthoclase, Fig. 16. The inner, central part is more crystalline with abundant gas cavities containing slightly corroded fayalites, bundles of aenigmatite and stubby or flaky crystals of arfvedsonite. The feldspar in the central part is a K-feldspar of variable composition, Fig. 16. Some very small Fe-hedenbergites are thought to belong to the groundmass crystallization, but may also be microphenocrysts.

Compositions of the various phases are given in Table IX. The fayalite lacks both a forsterite and a larnite component. The arfvedsonite is rather aluminous and manganoan, but low in calcium when compared to the arfvedsonites reported from the oversaturated, peralkaline rocks of Mayor Island (Nicholls & Carmichael, 1969) and the younger granites from Nigeria (Borley, 1963). The aenigmatite composition is almost identical to that of a groundmass aenigmatite reported from the comenditic lavas of Mt. Edziza, Canada (Yagi & Souther, 1974). It is rather low in TiO_2 and contains a ferri-aenigmatite component (Larsen, 1978).

The assemblage aenigmatite-fayalite to aenigmatite--arfvedsonite-fayalite places some constraints upon the conditions of formation, as illustrated in Fig. 17, where the buffer lines have been adopted directly from Nicholls & Carmichael (1969). However, Lindsley (1971) showed that the maximum stability for Ti-aenigmatite probably lies around the NNO buffer, and Ernst (1962) showed that Ti-free ferri-aenigmatite only exists under very reduced conditions (iron-wüstite buffer). The fact that arfvedsonite is present in the crystalline core of 19337, but not in the spherulitic rim implies that the final temperature during crystallization must have been close to the point where fayalite-aenigmatite and arfvedsonite coexist, approximately at 630°C and an fO_2 of 10^{-21}, (the thermal stability of arfvedsonite will be extended by substitution of OH by F, as is probably the case here). The low fO_2 is further emphasized by the low acmite component in the coexisting pyroxenes, where most of the acmite is present as a NAT-component (Rønsbo et al., 1977), Fig. 12.

THE XENOLITHS

The xenoliths can be divided into three groups:

1) cognate granophyres (10%)
2) altered plutonic and volcanic fragments (80%)
3) fresh volcanic fragments (10%).

The cognate granophyres constitute a range of types found as blocks up to 20 cm in diameter, but common to all of them are that they are massive, show well developed joint-surfaces, have fresh or only slightly altered mafic and leucocrate minerals, and are chemically and mineralogically closely related to the ignimbrite.

The altered plutonic and volcanic rocks show a wide range of types, ranging from porphyritic basalts over unporphyritic types and hyaloclastites to trachytic-textured basaltic-andesites and felsitic rhyolites, as well as strongly altered gabbros and granophyres. All the rocks show varying degrees of alteration, from zeolite and chlorophaeite vesicle-fillings, usually accompanied with abundant oxidation, through chloritization and sericitisa-tion, to rock fragments which mainly consist of pistacie-
-green epidote, ferri-actinolite and grossular, and have lost any original igneous texture.

The fresh volcanic fragments consist of the glassy rhyolite with microlites, mentioned earlier (Table IV), abundant palagonite tuff fragments, and very commonly a pilotaxitic aphyric basalt. Less common is a porphyritic basalt with unaltered phenocrysts of olivine, pyroxene and plagioclase.

PETROGENETIC CONSIDERATIONS

The use of mineral-glass equilibria, sequence of crystallization as well as general considerations can help to estimate some of the physical conditions of formation for the magma.

Estimation of P and T

The coexistence of magnetite and ilmenite allows an estimate of the magmatic temperature of the ignimbrite (Buddington & Lindsley, 1964; Powell & Powell, 1977), while the coexistence of glass and plagioclase feldspar can also be used as a geothermometer (Kudo & Weill, 1970).

As the compositional variation of the magnetites is comparatively large within the single samples, the extreme values rather than an average have been used to determine a range of temperatures and oxygen-fugacities for a number of samples, Table XII, Fig. 17. The temperatures obtained are high when compared with temperatures obtained from other rhyolites (Carmichael, 1967), though some authors suggest similar temperatures (Lerbekmo et al., 1975; Coulon et al., 1978). Several explanations are possible for the high temperatures. (1) The temperatures are on the limit of and above the experimental data of Buddington & Lindsley (1964) upon which the thermometer is based. (2) The oxide phases did not equilibrate. This may be the case at least in the lower part of the ignimbrite, where magnetite apparently was not a stable phase at the time of extrusion. (3) Some external factor may have affected the Fe-Ti oxides, possibly the invasion of basic magma into the acid magma-chamber, which heated the acid body and caused the oxides to reequilibrate.

The temperatures of plagioclase rims in equilibrium with the surrounding glass have been calculated for four samples at different PH_2O, using the equations of Kudo & Weill (1970), in addition temperatures for cores and intermediate positions have been calculated for 2 samples. All results are presented in Table XIII. In view of the temperatures obtained by the same method on various other rhyolites (Stormer & Carmichael, 1970), the results for the rims do not appear unreasonable (the increasing temperatures at pressures .5 kb are due to arbitrary roots in the equations). The results must, however, be treated

with great care as several factors may affect the results drastically. (1) Kudo & Weill (1970) warned against the use of the thermometer outside the An_{90}-An_{10} range because of the large sensitivity for small compositional changes beyond these limits. (2) The large orthoclase component present is unaccounted for in the original equations of Kudo & Weill (1970). (3) The liquid was peralkaline and thus had a structure different from that of the peraluminous liquids upon which the thermometer is based. This last effect is very difficult to evaluate, but the crystallization path of the feldspars does not show any influence of the "orthoclase" effect (Bailey & Schairer, 1964) commonly found in peralkaline rocks and whose appearance is attributed to the changed structure of the melt.

In spite of the large uncertainities involved in the temperature estimates presented above, these have been compared in Fig. 18, and it is apparent that there is an increase in the Fe-Ti oxide temperatures with increasing stratigraphic height, and an increasing departure from the line of equal temperature for the thermometers, which may be the result of heating of the magma-chamber by intrusion of basic material into it during the eruption, with resulting reequilibration of the Fe-Ti oxides, as evidenced by the anomalous Fe-Ti oxide relationships in sample 22042.

Sample 19342h is a feldspar microcryst from the low silicic component of a hybrid fiamme which is supposed to represent crystallization in the vent or in the eruption column, and the temperature thus the eruption temperature. If this temperature is combined with a coexisting ilmenite, Table X, a fO_2 of $10^{-13.3}$ can be deduced from the Buddington & Lindsley (1964) tables. This is slightly above the FMQ-buffer, Fig. 17.

The difference in feldspar compositions between samples 19337 and 22042, Fig. 7, may be taken as a confirmation of that the calculated difference in feldspar temperatures illustrated in Fig. 18, is real and not a function of accumulated errors, and thus is in accordance with the experiments

of Seck (1971) who showed that the curve of evolution in the system An-Ab-Or-H_2O shifted towards the Ab corner with decreasing temperature. This implies that a thermal gradient did exist in the magma-chamber(s). This gradient was probably responsible for the resorption and oscillatory zoning observed, probably by convective movement of the phenocrysts in the boundary layer towards the crystallizing granophyre sheath.

The decreasing Al content in the pyroxenes, Fig. 11, may also be a function of decreasing temperature (Kushiro, 1962; Thompson, 1974; Herzberg, 1978), but in this case related to the overall cooling of the magma during crystallization, as the change is not stratigraphically related. This overall cooling was apparently accompanied by a decrease in fO_2, stabilizing a NAT-component (Rønsbo et al., 1977) at the expense of the previously stable Ca-Ti-Tschermaks component, Fig. 12. The decrease in temperature and fO_2 brought fayalite on the liquidus in the upper part of the magma-chamber, and probably resulted from a reaction of the type:

$$\underset{\text{magnetite}}{2/3\ Fe_3O_4} + \underset{\text{glass}}{SiO_2} \quad \underset{\text{fayalite}}{Fe_2SiO_4} + \underset{\text{vapor}}{1/3\ O_2}$$ (Nicholls et al., 1971)

to become active at the expense of the magnetite crystallization.

Magmatic evolution

The inclusion pattern, as well as the relative abundance and composition of the phenocrysts can be used to give some implication of the evolution of the magma. Fig. 19 shows the crystallization sequence of the magma is deduced from the inclusion pattern. The estimate of crystallinity is based on the absolute amount of phenocrysts of the specific composition (+older cores) present today. The figure shows that most of the minor minerals did not crystallize until late in the evolution of the magma.

The plagioclase geothermometry, Table XIII, indicated that the interior of the larger feldspar phenocrysts were not in equilibrium with the glass, and thus implies that they must have developed in a liquid of a different composition. A suitable parent composition is found in the low silicic liquid presented in Table IV, as further supported by plots in the feldspar composition diagram of Bailey & Macdonald (1970), Fig. 20. Table XIV shows the results of a fractionation calculation, using the low silicic composition as parent. It gives a reasonable fit, but the fractionated amount is twice the observed crystallinity implying that a considerable amount of crystals must have been removed. The cognate granophyres mantling the magma-chamber, and now found as xenoliths in the ignimbrite, may well account for the missing fractionate.

The present study throws no light on the possible origin of the low silicic composition, but as it is similar in composition to many other Icelandic rhyolites (rhyodacites) the reader is referred to the works of Sigvaldason (1974), Sigurdsson (1970, 1977), Grönvold (1972) and Johannesson (1975) for possibilities.

The origin of the high silicic composition, Table IV, is obscure as the feldspar composition diagram, Fig. 20, clearly shows that it can neither have been derived from the low silicic composition nor from the "normal" rhyolitic composition solely by fractional crystallization, thus some other process must be invoked.

Depth of the magma-chamber

The considerations above indicate some characteristics of the general behaviour of the magma, but nothing about the depth to the magma-chamber. An estimate of this can be made by using two approaches, the first by matching the liquid with experiments, the other by comparison to known intrusions of comparable rocks. As the normative composition of the rhyolite is only very slightly peralkaline, and

does not possess an anorthite component, then it can be treated in the granite system of Tuttle & Bowen (1958), Fig. 21. From this it is apparent that the rhyolite cannot have been subjected to water pressures higher than 1500-2000 bars, otherwise quartz would have been present. This corresponds to a maximum depth of 5-8 km, provided $P_t = PH_2O$, (if not then the figure increases). Assuming the lowest Fe-Ti oxide temperature to be correct, then the plagioclase geothermometer, Table XIII, indicates that PH_2O probably never reached 1000 bars, thus explaining why the results for this pressure are arbitrary roots. The indication that the eruption started with an effusive phase, on the other hand implies that the magma originally was not saturated with volatiles, and that vesiculation (volatile exsolution) did not start until an open conduit to the surface had been established.

Another approach is indirect, by comparing xenoliths of the surrounding granophyre mantle with rocks from known intrusions of comparable chemistry. One striking difference here is the near absence of miarolitic cavities in the xenoliths, as such are common in the Austurhorn intrusion (Blake, 1966) and abundant in the shallow Urdarfell intrusion (Annells, 1968). Wager et al. (1965) describes the cavities as characteristic of shallow level intrusions where the internal vapor pressure at times exceed the external pressure. In the case of the Austurhorn intrusion Blake (1966) on stratigraphic reasons estimates the top of the intrusion to have been at a depth of 1700 m at the time of emplacement. The thickness of the intrusion exposed is 750 m and miarolitic throughout. This probably places an upper limit for emplacement of the Thorsmörk granophyres at 2.5-3 km depth. In other words, it seems reasonable to expect the magma-chamber to have resided at a depth between 3 and 8 km, a range which includes the boundary between the seismic layers 2 and 3 in the area, (Palmason, 1971). The low estimated PH_2O as well as the granophyric texture, which needs a comparatively steep thermal gradient towards

he country rock to develope, makes it probable that the actual depth was closer to the 3 km than to the 8 km.

In Fig. 22 a speculative reconstruction is presented showing the emplacement of a laccolithic body with a geometric size of 8 km^3 (the maximum volume estimate for the eruption). The shape has mainly been selected as a matter of convenience, a stock or cedar tree form are just as possible. This was situated in the boundary region between layers 2 and 3, taking into account the bell-shaped boundary between these layers found by Palmason (1971) beneath other central complexes. The width of the intrusion is thought to be confined within the caldera perimeter faults of the central complex.

SUMMARY OF CONCLUSIONS

The Thorsmörk ignimbrite represents the products of one of the largest acid eruptions in Iceland.

The textures of the acid glass suggests that the eruption started comparatively quietly, possibly even with an effusive phase, but through a phreatomagmatic phase increased in explosivity to a cataclysmic event that produced a thick, xenolith-rich deposit, after which the eruption declined with a few final vigorous outbursts.

The eruption probably started at a restricted vent that rapidly developed into a fissure from which tephra of diffent compositions was ejected from the central parts to form a series of pyroclastic flows, while the distal parts of the fissure probably produced basaltic lavas through strombolian to hawaiian activity. The activity probably shifted along the fissure with time, with only the rhyolitic segment as a permanent, and all-dominating member.

At the time of eruption the magma-chamber was an old feature with a well developed contact aureole and a thick envelope of granophyre, and abundant phenocrysts in the magma-chamber. Originally it was a low silicic rhyolite

(rhyodacite) but fractional crystallization had changed it into a slightly peralkaline rhyolite, with a silicic cap of an even more peralkaline rhyolite.

During the crystallization the temperature and the oxygen fugacity in the magma decreased, while at the same time a minor temperature gradient existed between top and bottom, resulting in fayalite coming on the liquidus only in the upper part of the magma-chamber before the eruption.

In connection with the eruption the acid magma was intruded by basic magma that mixed with the acid magma forming a range of hybrid compositions, and raising the temperature and oxygen fugacity of the remaining acid magma.

ACKNOWLEDGEMENTS

This study was initiated while the author was a student at the University of Copenhagen, and all field work paid by that institution.

All laboratory work was conducted while the author held a fellowship at the Nordic Volcanological Institute, Iceland. The present manuscript has benefitted strongly from criticism and discussion with G.E. Sigvaldason, K. Grönvold, G. Larsen and P.O. Mørkeseth, Reykjavik and A.K. Pedersen, L.M. Larsen and C.K. Brooks, Copenhagen.

Special thanks goes to H. Bollingberg, Copenhagen, for the spectrographic analyses, and to V. Poulsen, Copenhagen, for the excellent thin sections of a very difficult material.

REFERENCES

Annels, R.N., 1968. A geological investigation of a tertiary intrusive centre in the Vididalur-Vatnsdalur area, northern Iceland. Ph.D. thesis, University of St. Andrews.

Bailey, D.K. and Macdonald, R., 1970. Petrochemical variations among mildly peralkaline (comendite) obsidians from the oceans and continents. Contr. Mineral. and Petrol. 28, 340-351.

Bailey, D.K. and Schairer, J.F., 1964. Feldspar liquids equilibria in peralkaline liquids: The orthoclase effect. Am. J. Sci. 262, 1198-1206.

Baker, P.E., Buckley, F. and Holland, J.G., 1974. Petrology and geochemistry of Easter Island. Contr. Mineral. and Petrol. 44, 85-100.

Bence, A.E. and Albee, A.L., 1968. Empirical correction factors for the electron microanalysis of silicates and oxides. J. Geol. 76, 382-403.

Bennett, F.D., 1974. On volcanic ash formation. Am. J. Sci. 274, 648-669.

Blake, D.H., 1966. The netveined complex of the Austurhorn intrusions of southeastern Iceland. J. Geol. 74, 891-907.

Borley, G.D., 1963. Amphiboles from the Younger Granites of Nigeria. Part I. Chemical classification. Min. Mag. 33, 358-376.

Bowles, J.F.W., 1977. An estimation of the probable errors of the method of tracing the cooling history of complex magnetite-ilmenite grains and a discussion of the results produced by using different methods of treatment of the minor elements contained in these minerals when using the Buddington and Lindsley (1964) geothermometer. Min. Mag. 41, M16.

Buddington, A.F. and Lindsley, D.H., 1964. Iron-titanium oxide minerals and synthetic equivalents. J. Petrol. 5, 310-357.

Cailleux, A., 1978. Niveo-eolian deposits. Pp. 501-503 in R.W. Fairbridge and J. Bourgeois (eds.) The encyclopedia of sedimentology. Dowden, Hutchinson and Ross, U.S.A.

Carmichael, I.S.E., 1964. The petrology of Thingmuli, a Tertiary volcano in eastern Iceland. J. Petrol. 5, 435-460.

Carmichael, I.S.E., 1967. The iron-titanium oxides of salic volcanic rocks and their associated ferro-magnesian silicates. Contr. Mineral. and Petrol. 14, 36-64.

Coulon, C., Dostal, J. and Dupuy, C., 1978. Petrology and geochemistry of the ignimbrites and associated lava domes from N.W. Sardinia. Contr. Mineral. and Petrol. 68, 89-98.

Ernst, W.G., 1962. Synthesis, stability relations and occurrence of riebeckite-arfvedsonite solid solutions. J. Geol. 70, 689-736.

Grönvold, K., 1972. Structural and petrochemical studies in the Kerlingarfjöll region, central Iceland. Ph.D. thesis, Oxford. 236 pp.

Guppy, E.M. and Hawkes, L., 1925. A composite dyke from eastern Iceland. Quart. J. Geol. Soc. Lond. 81, 325-341.

Heiken, G.H., 1972. Morphology and petrography of volcanic ashes. Geol. Soc. Am. Bull. 83, 1961-1988.

Heiken, G.H. and Eichelberger, J.C., 1980. Eruptions at Chaos Crags, Lassen Volcanic National Park, California. J. Volc. Geoth. Res. 7, 443-481.

Herzberg, C.T., 1978. Pyroxene geothermometry and geobarometry: Experimental and thermodynamic evaluation of some subsolidus phase relations involving pyroxenes in the system $CaO-MgO-Al_2O_3-SiO_2$. Geochim. Cosmochim. Acta 42, 945-958.

Imsland, P., 1978. The petrology of Iceland. Some general remarks. Nordic Volcanological Institute, report 7808.

Jaffe, H.W., Evans, H.T. and Chapman, R.W., 1956. Occurrence and age of chevkinite from the Devil´s slide fayalite-quartz syenite near Stark, New Hampshire. Am. Min. 41, 474-487.

Jakobsson, S.P., 1972. Chemistry and distribution pattern of recent basaltic rocks in Iceland. Lithos 5, 365-386.

Johannesson, H., 1975. Structure and petrochemistry of the Reykjadalur central volcano and the surrounding areas, midwest Iceland. Ph.D. thesis, Durham University, 273 pp.

Jørgensen, K.A., in press. The Thorsmörk ignimbrige: An unusual comenditic pyroclastic flow from southern Iceland. J. Volc. Geoth. Res.

Kudo, A.M. and Weill, D., 1970. An igneous plagioclase thermometer. Contr. Mineral. and Petrol. 25, 52-65.

Kushiro, I., 1962. Clinopyroxene solid solutions. Part I. The $CaAl_2SiO_6$ component. Japan J. Geol. Geogr. 33, 213-220.

Larsen, G. and Thorarinsson, S., 1977. H_4 and other acid Hekla tephra layers. Jökull 27, 28-46.

Larsen, L.M., 1977. Aenigmatites from the Ilimaussaq intrusion, south Greenland: Chemistry and petrological implications. Lithos 10, 257-270.

Lerbekmo, J.F., Westgate, J.A., Smith, D.G.W. and Denton, G.H., 1975. New data on the character and history of the White River volcanic eruption, Alaska, Pp. 203-209 in R.P. Suggate and M.M. Cresswell (eds.) Quaternary studies. Roy. Soc. New Zealand, Wellington.

Lindsley, D.H., 1971. Synthesis and preliminary results on the stability of aenigmatite ($Na_2Fe_5TiSi_6O_{20}$). Carn. Inst. Ann. Rep. Geophys. Lab. 69, 188-190.

McBirney, A.R., 1973. Factors governing the intensity of explosive andesitic eruptions. Bull. Volc. 37, 443-453.

Meyer, J.D., 1972. Glass crust on intratelluric phenocrysts in volcanic ash as a measure of eruptive violence. Bull. Volc. 35, 358-368.

Nicholls, J. and Carmichael, I.S.E., 1969. Peralkaline acid liquids: A petrological study. Contr. Mineral. and Petrol. 20, 268-294.

Nicholls, J., Carmichael, I.S.E. and Stormer, J.C., 1971. Silica activity and P_{total} in igneous rocks. Contr. Mineral. and Petrol. 33, 1-20.

Palmason, G., 1971. Crustal structure of Iceland from explosion seismology. Soc. Sci. Isl. 40, 180 pp.

Powell, R. and Powell, M., 1977. Geothermometry and oxygen barometry using coexisting iron-titanium oxides: A reappraisal. Min. Mag. 41, 257-264.

Rønsbo, J.G., Pedersen, A.K. and Engell, J., 1977. Titan-aegirine from early Tertiary ash-layers in northern Denmark. Lithos 10, 193-204.

Seck, H.A., 1971. Koexistierende Alkali-Feldspäte und Plagioklase im System $NaAlSi_3O_8$-$KAlSi_3O_8$-$CaAl_2Si_2O_8$-H_2O bei Temperature von 650°C bis 900°C. N. Jbh. Min. Abh. 115, 315-395.

Segalstad, T.V. and Larsen, A.O., 1978. Chevkinite and perrierite from the Oslo region, Norway. Am. Min. 63, 499-505.

Sigurdsson, H., 1970. Petrology of the Setberg volcanic region and the acid rocks of Iceland. Ph.D. thesis, Durham University, 321 pp.

Sigurdsson, H., 1977. Generation of Icelandic rhyolites by melting of plagiogranites in the oceanic layer. Nature 269, 25-28.

Sigvaldason, G.E., 1974. The petrology of Hekla and the origin of silicic rocks in Iceland. The Eruption of Hekla 1947-48. Soc. Sci. Isl. V, 1-44.

Sparks, R.S.J., 1978. The dynamics of bubble formation and growth in magmas: A review and analysis. J. Volc. Geoth. Res. 3, 1-38.

Sparks, R.S.J. and Wilson, L., 1976. A model for the formation of ignimbrite by gravitational column collapse. J. Geol. Soc. Lond. 132, 441-451.

Stormer, J.C. and Carmichael, I.S.E., 1970. The Kudo-Weill plagioclase geothermometer and porphyritic acid glasses. Contr. Mineral. and Petrol. 28, 306-309.

Sæmundsson, K., 1972. Jardfrædiglefsur um Torfajökulssvædid. Natturufrædingurinn 42, 81-99 (in Icelandic).

Sæmundsson, K., 1978. Fissure swarms and central volcanoes of the neovolcanic zones of Iceland. Pp. 415-432 in D.R. Bowes and B.E. Leake (eds.) Crustal evolution in northwestern Britain and adjacent regions. Geol J. Spec. Issue 10.

Thompson, R.N., 1974. Some high-pressure pyroxenes. Min. Mag. 39, 768-787.

Thorarinsson, S., 1969. Ignimbrit i Thorsmörk. Natturufrædingurinn 39, 139-155 (in Icelandic).

Tröger, W.E., 1971. Optische Bestimmung der gesteinsbildenden Minerale. Teil 1, 4. Auflage. Schweizerbart´sche Verlagsbuchhandlung, Stuttgart, 188 pp.

Tuttle, O.F. and Bowen, N.L., 1958. Origin of granite in the light of experimental studies in the system $NaAlSi_3O_8$-SiO_2-H_2O. Geol. Soc. Am. Mem. 74, 153 pp.

Wager, L.R., Vincent, E.A., Brown, G.M. and Bell, J.D., 1965. Marscoite and related rocks of the Western Red Hills Complex, Isle of Skye. Phil. Trans. Roy. Soc. Lond. Ser. A. 257, 273-307.

Walker, G.P.L. and Croasdale, R., 1972. Characteristics of some basaltic pyroclastics. Bull. Volc. 35, 303-317.

Wetzel, R., Wenk, E., Stern, W. and Schwander, H., 1978. Beiträge zur Petrographie Islands. Publ. Stift. Vulk. Inst. Im. Friedländer 10, 128 pp.

Wright, T.L. and Doherty, P.C., 1970. A linear programming and least squares computer method for solving petrologic mixing problems. Geol. Soc. Am. Bull. 81, 1995-2008.

Yagi, K. and Souther, J.G., 1974. Aenigmatite from Mt. Edziza, British Columbia, Canada. Am. Min. 59, 820-829.

Table I. General Sample Data

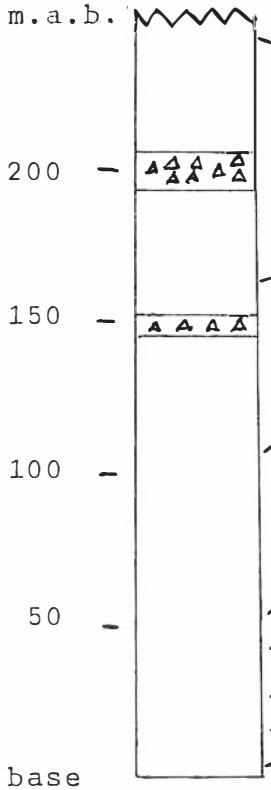

Sample no.	Modal proportions (estimated). Phenocryst %	Xenolith %	B.gl.[1]	Int.gl.[2]	Fayalite	Welding
22042	15	20	0	3	<.1	none
30474	5	7	12	0	<.1	none
30476	7	15	5	.5	.1	none
19416	12	20	5	.5	.3	none
19342	22	10	3	1	.4	moderate
19420	7	2	1		.3	moderate
19337	15	1	<.5		.5	strong
30483	5	20	2	.2	+	none

1) B.gl. = Basic glass in modal %.

2) Int.gl. = Intermediary glass in modal %.

ΔΔΔ = Xenolith rich horizons in composite stratigraphic column.

Table II. Characteristic features of the acid tephra

Sample	30483	19416	30474	22042
Pumice				
vesicle shape	regular	regular	irregular	irregular
vesiculation[1)]	10 - 80%	25 - 80%	40 - 80%	60 - 80%
vesicle size µm	10-30 5-60	10-20 30-150	10-60 5-300	.5-500 2-150
wall size µm	30-60 1-10	5-20 .2-10	5-40 1-20	1-20 .4-30
Pipe vesicles				
size order µm	5 - 10	1 - 5	4 - 60	1 - 4
abundance[2)]	50%	30%	50%	10%
Radial vesicles				
size order µm	20	÷	30	÷
abundance[3)]	10%		40%	
Shards				
shape	equant + Y	Y	Y	star
size range µm	100 - 1000	100 - 600	100 - 600	100 - 1000
Abrasion Index[4)]				
range	100 - .7	100 - 4	100 - 1	100 - 5.6
average	10	19	10	50

Explanation: 1) % voids per surface area of pumice clasts phenocrysts.

2) % pipe vesicles of all pumice clasts, expressed as surface area.

3) % phenocrysts in pumices with radial vesicles.

4) $\frac{\%\ \text{crystal}}{\%\ \text{glass}}$ of discrete phenocrysts (feldspar) (Meyer, 1972).

Table III. Summary of eruptive events

Phase	Event	Evidence
effusive	formation of acid coulée	angular fragments of glassy rhyolite in lowermost part of ign.
initial explosive	phreatomagmatic activity	equant shards of "normal" rhyolite, little vesiculated pumice clasts
developing	repeated discharge of pyroclastic flows, overall increase in explosivity	multiple flow units with minor breaks increasing abundance of lithic bands increasing vesicularity and abrasion index
culminating	cataclysmic event	major xenolithic unit with abundant mixed pumice clasts
declining	intermittent discharge of pyroclastic flows, with high explosivity and increasing repose periods	flow units with strongly vesiculated clasts and shards and intercalated sediments

Table IV. The rhyolitic glasses

	1	2	3	4
Type	xenol.	low Si	av. Si	high Si
SiO_2	69.08	71.03	74.28	75.17
Al_2O_3	13.48	13.14	11.41	11.69
TiO_2	.38	.26	.17	.18
FeO^t	4.32	3.25	2.73	2.79
MnO	.16	.17	.07	.06
MgO	.08	.05	.02	.02
CaO	1.28	1.20	.42	.32
Na_2O	5.23	5.31	4.82	4.53
K_2O	3.43	3.54	4.17	5.24
P_2O_5	.06	.03	.01	.01
Sum	97.50	97.98	98.10	100.01
F			.02	.14
Cl			.30	.25
CIPW norms with fixed Fe^{3+}/Fe^t = .15				
Qz	21.58	23.33	31.09	30.19
Or	20.90	21.34	25.11	30.95
Ab	45.63	45.84	36.15	30.94
An	1.21	1.60		
Ac			1.06	1.37
Ns			.98	1.35
Di	4.37	3.80	1.83	1.35
Hy	4.53	3.00	3.43	3.48
Mt	.87	.64		
Il	.74	.50	.33	.34
Ap	.14	.07	.02	.02
Selected trace elements in ppm				
Ba		460	460	760
Sr		190	45	28
Ga		25	22	23
V		82	15	<10
Zr		765	935	950
Y		40	145	105
Nb		69	90	105
La		75	85	91

Major elements by microprobe analyses. Trace elements by emission spectrography by H. Bollingberg, Copenhagen. The trace elements in no. 3 are inferred from whole rock analyses.

1) Sample 19416. Microlithic, glassy rhyolite fragment. Average of 2 analyses.

2) Sample 19416. Homogenous grey glass clast. Average of 3 analyses.

3) Average of all shard analyses, n=22.

4) Sample 19337. Average of 12 analyses of homogenous glass rim.

Table V. Characteristic features of the feldspars

Type	1	2	3
Max. size in mm	5	2	.1
Habit	tabular	elongate	stubby
Twinning	complex	simple	(simple)
" laws[1]	K,A,P,B	K,A	(K)
Resorp/Exsol[2]	occasional	rare	÷
Modal %[3]	50	50	>1
Numerical %[4]	15 (range 11-25)	83	2
Comp. range core	$An_{10}Ab_{81}Or_9$	$An_5Ab_{82}Or_{13}$	$An_2Ab_{78}Or_{20}$
Comp. range rim	$An_2Ab_{81}Or_{17}$	$An_2Ab_{81}Or_{17}$	$An_2Ab_{78}Or_{20}$

Explanation:

1) K,A,P,B; Carlsbad, Albite, Pericline and Baveno respectively.

2) Resorption and/or exsolution present.

3) % of total feldspar area.

4) % of total number of feldspars.

Table VI. Representative feldspar analysis

	core	intm.	rim	micro.	mic.h.	quench
SiO_2	68.81	69.66	67.03	70.00	67.58	68.14
Al_2O_3	20.92	20.55	19.67	19.25	17.71	18.57
FeO^t	.28	.24	.31	.42	.90	.77
CaO	2.15	1.16	.25	.30	.32	.93
Na_2O	9.90	9.46	9.23	9.11	7.70	9.27
K_2O	1.47	2.34	2.99	3.27	3.12	1.46
Sum	103.52	103.41	99.49	102.34	97.45	99.23
Formulas based on 32 oxygens						
Si	11.73	11.87	11.90	12.07	12.20	12.06
Al	4.20	4.13	4.12	3.91	3.77	3.88
Fe	.04	.03	.05	.06	.14	.11
Ca	.39	.21	.05	.06	.14	.11
Na	3.27	3.13	3.18	3.04	2.70	3.18
K	.32	.51	.68	.72	.72	.33
Modal						
An	9.8	5.5	1.2	1.4	1.8	4.8
Ab	82.1	81.3	81.4	79.7	77.5	86.3
Or	8	13.2	17.3	18.8	20.7	9

(All analyses from sample 19342)

Table VII. Characteristic features of the pyroxenes

Type	1	2	3
Max. size mm.	2	.5	.1
Habit	stubby	elongate	equant (skeletal)
Shape	subhedral	euhedral	euhedral
Inclusions	abundant	rare	-
Modal %[1]	15	80	5
Mg range (formula un.)	.09-.03	.05-.02	.018

1: of pyroxenes present

Table VIII. Representative pyroxene analyses

Sample	19359T				19342			22154				30483
Type	core	rim	core	rim	rod in fsp.	microh.	quench	core1 zonar	core2 px. group	mantle	rim	res. in acid gl.
SiO_2	47.83	46.81	47.82	48.18	45.89	46.61	46.92	50.82	48.36	47.23	46.99	49.28
Al_2O_3	.49	.32	.39	.27	.36	.98	.83	.51	.51	.32	.50	.95
TiO_2	.38	.29	.33	.30	.38	1.22	.68	.06	.32	.44	.37	.69
FeO^t	29.78	30.14	30.16	30.60	31.04	30.09	32.16	17.53	23.59	30.67	29.51	20.97
MnO	1.18	1.21	1.29	1.24	1.25	1.29	1.64	1.20	1.07	1.26	1.15	.80
MgO	1.15	.49	.69	.26	.13	.42	.48	8.76	4.75	.40	.52	6.85
CaO	19.94	19.80	19.88	19.61	18.31	18.52	16.14	20.99	20.28	19.37	18.28	20.26
Na_2O	.45	.46	.47	.57	.47	.48	.41	.39	.40	.46	1.22	.33
Sum	101.21	99.52	101.01	101.04	97.82	99.63	99.26	100.25	97.36	100.15	98.57	100.14
Formulas based on 6 oxygens												
Si	1.941	1.941	1.950	1.969	1.946	1.935	1.965	1.965	1.946	1.949	1.951	1.939
Al	.023	.016	.019	.013	.018	.048	.041	.023	.024	.016	.024	.044
Ti	.012	.009	.010	.009	.012	.038	.021	.002	.010	.014	.012	.020
Fe^{3+}	.106	.121	.098	.075	.105	.044	.019	.072	.096	.094	.150	.063
Fe^{2+}	.905	.924	.931	.971	.996	1.001	1.108	.495	.698	.964	.874	.627
Mn	.041	.042	.045	.043	.045	.045	.058	.039	.036	.044	.040	.027
Mg	.070	.030	.042	.016	.008	.026	.030	.505	.285	.025	.032	.402
Ca	.867	.880	.869	.859	.832	.824	.724	.870	.874	.856	.813	.854
Na	.035	.037	.037	.045	.039	.039	.033	.029	.031	.037	.098	.025
Mol %												
Ca	46.5	45.0	44.8	44.7	42.9	43.5	38.5	44.8	44.8	44.2	43.5	43.9
Mg	3.6	1.5	2.1	.8	.4	1.4	1.6	26.0	14.6	1.3	1.7	20.7
Fe	51.9	53.5	53.1	54.5	56.7	55.1	59.9	29.2	40.7	54.6	54.8	35.5

Type explanation: The first 4 analyses are two sets of analyses (core-rim) covering the whole normal spectrum of pyroxenes observed in the ignimbrite. Rod in fsp. is a pyroxene rod in a feldsparphenocryst in the hybrid fiamme. Microh. is a microphenocryst from the same hybrid fiamme. Q is an acicular pyroxene in a acid quench clot. The analyses from 22154 are all from the mantled pyroxene group mentioned in the text. The analysis from 30483 is a light yellow resorbed pyroxene in acid glass. Fe^{2+}/Fe^{3+} distribution based on stoichiometry with 4 cations and 6 oxygens.

Table IX. Minor minerals (partial analyses)

	Apatite	Zircon	Chevkin.	Fayalite
SiO_2	.84	33.36	19.14	30.28
Al_2O_3	0	.03	.22	0
TiO_2	.03	0	20.83	.04
FeO^t	.64	.84	11.80	67.41
MnO	.14	.08	0	3.01
MgO	.01	0	.01	.16
CaO	53.69	.06	3.91	.38
Na_2O	.13	.02	0	0
P_2O_5	41.39	.05	0	0
Sum	96.87	34.43	55.91	101.28

Table X. Representative oxide analyses

No.	1	2	3	4	5	6	7	8	9	10	11
Phase	rhombohedral						spinel				
SiO_2	.14	.06	.07	.06	.03	.16	.28	.59	.18	1.31	.42
Al_2O_3	.01	.01	.05	.02	.03	.00	.44	.48	.36	.37	0
TiO_2	48.24	49.30	46.47	50.06	46.58	46.81	22.11	22.20	18.53	27.82	19.72
FeOt	50.08	48.59	48.46	49.10	51.03	46.50	70.40	70.04	75.74	65.42	78.24
MnO	1.42	1.50	1.38	1.74	1.74	1.99	1.15	1.04	1.00	1.05	1.03
MgO	.00	.03	.04	.01	.02	.02	.03	.05	.02	.03	.04
CaO	.61	.00	.08	.02	.02	.00	.53	.09	.05	.08	.59
Cr_2O_3	.01	.00	.00	.02	.02	.00	.00	.00	.01	.05	.01
V_2O_3	.18	.12									
NiO	.08	.00									
ZnO	.00	.13									
Sum	100.77	99.74	96.55	101.01	99.68	95.50	94.93	94.49	95.89	94.14	100.05
Formula based on 6 oxygens							32 oxygens				
Si	.007	.003	.004	.003	.002	.008	.086	.183	.055	.401	.123
Ti	1.805	1.870	1.817	1.875	1.764	1.853	5.124	5.172	4.243	6.059	4.326
Al	.001	.001	.003	.001	.002	.000	.160	.175	.129	.133	0
Cr	.000	.000	.000	.001	.001	.000	.000	.000	.002	.012	.002
Fe^{3+}	.368	.248	.355	.242	.461	.277	5.422	5.118	7.274	2.916	7.103
Fe^{2+}	1.716	1.802	1.752	1.804	1.689	1.770	12.718	13.026	12.012	14.150	11.981
Mn	.060	.064	.061	.073	.074	.089	.300	.273	.258	.072	.254
Mg	.000	.002	.003	.001	.002	.002	.014	.023	.009	.014	.026
Ca	.033	.000	.004	.000	.000	.001	.175	.030	.016	.026	.184
Mol proportions											
Ilm	90.3	93.5	90.8	93.7	88.0	92.7	Usp 68.1	70.2	56.0	84.6	57.5
Hm	9.7	6.5	9.2	6.3	12.0	7.3	Mt 31.9	29.8	44.0	15.4	42.5

Calculation of Fe^{2+} and Fe^{3+} based on stoichiometry (Carmichael, 1967). Ulvoespinel-magnetite prop. after subtraction of Jacobsite, $MnFe_2O_4$, from analysis.

Explanation:

1) Sample 19337, ilmenite xenocryst.
2) Sample 19337, ilmenite phenocryst.
3) Sample 22042, ilmenite phenocryst.
4) Sample 19342, skeletal phenocryst, core.
5) Sample 19342, skeletal phenocryst, rim.
6) Sample 19342, microcryst in hybrid fiamme.
7) Sample 19337, magnetite inclusion in px.
8) Sample 22042, magnetite inclusion in px.
9) Sample 22154, inclusion in fsp in zonar px mp.
10) Sample 22154, incl. in glass incl. in zon. px.
11) Sample 19342, acicular mt in acid quench clot, after subtraction of 22% anorthoclase from analysis.

Table XI. Groundmass phases from sample 19337

	Sanidine	Anorthoclase	Fe-Hedenbergite	Fayalite	Arfvedsonite	Aenigmatite
SiO_2	68.98	73.77	46.54	29.65	46.95	40.26
Al_2O_3	14.70	13.37	.27	0	2.74	.41
TiO_2			.51	.08	.80	7.25
FeO^t	1.54	1.20	30.93	67.16	37.32	45.26
MnO			1.23	3.07	2.07	.96
MgO			.12	0	.05	.06
CaO	.18	.06	18.79	0	.54	.30
Na_2O	5.38	6.69	.56		5.79	6.96
K_2O	6.41	2.85			1.38	.02
Sum	97.20	98.14	98.96	99.96	97.63	101.48

The anorthoclase analysis probably includes some tridymite.

Table XII. fO_2 temperatures deduced from Fe-Ti oxides

Sample	Temperature range °C		-log fO_2 range	
	1	2		
19337	955-1025	943-1033	12.0-10.6	11.9- 9.9
19420	920-1000	898- 960	12.6-11.0	12.8-11.3
19359T	930-1025	888- 964	12.3-10.6	12.9-11.1
22042	1035-1090	1018-1079	10.4- 9.9	10.1- 9.2

1) Graphically determined from tables of Buddington & Lindsley (1964), mole fractions calculated after method of Carmichael (1967).

2) Calculated after formulas of Powell and Powell (1977) mole fractions as suggested by Bowles (1977).

Table XIII. Plagioclase temperatures after Kudo & Weill (1970)

Sample	Temperature in °C at a H_2O pressure of			
	0 kb	.5 kb	1 kb	5 kb
19342 hybride	862	824	845	885
19337 rim	933	893	908	928
19420 core	794	768	817	906
19420 intermed.	777	719	760	894
19420 rim	948	908	921	936
22042 core	744	671	773	897
22042 intermed.	936	896	911	933
22042 rim	956	915	927	938

Table XIV. Fractionation model based on three minerals

	D	fsp	px	ilm	P	P_{calc}	diff.
SiO_2	74.28	65.01	47.60	.03	71.03	71.03	.00
Al_2O_3	11.41	19.67	.29	.02	13.14	12.98	.16
TiO_2	.17	.00	.38	48.57	.26	.20	.06
Fe_2O_3	.60	.28	1.59	7.36	.75	.56	.19
FeO	2.13	.00	29.56	42.38	2.25	2.36	-.11
MnO	.07	.00	1.18	1.24	.17	.08	.09
MgO	.02	.00	.33	.02	.05	.02	.03
CaO	.42	1.26	18.47	.03	1.20	1.06	.14
Na_2O	4.82	9.16	.46	.00	5.31	5.69	-.38
K_2O	4.17	2.29	.04	.00	3.54	3.61	-.07
$X_{fract.}$	.737	.232	.025	.001			

Explanation:

D = fractionated liquid (table IV, no. 3).

fsp, px, ilm = feldspar (sample 19420, phen core), pyroxene (sample 22042, phen core) and ilmenite (sample 19359T, phen) used in fractionation.

P = supposed parent liquid (table IV, no. 2).

P_{calc} = calculated parent liquid.

diff. = difference between P and P_{calc}.

$X_{fract.}$ = fractionated amount.

Calculation based on method of Wright and Doherty (1970).

FIGURE CAPTIONS

Fig. 1. Distribution map of the ignimbrite (random bars) showing sample locations (numbers). Stipple: alluvium. Triangles: prominent heights. Insert map shows location relative to the active zones of Iceland.

Fig. 2. Photomicrograph of pipe-vesicles distorted by radial vesicles. Bar length: 1 mm.

Fig. 3. Photomicrograph of star-shaped shard from 22042. Bar length: .25 mm.

Fig. 4. Photomicrograph of equant shard from 30483. To the right low vesiculated pumice (40%). Bar length: .25 mm.

Fig. 5. Oxide variation diagram for the major elements of the acid glasses. Filled circles: pumice analyses. Open circles: little vesiculated glasses from 30483. Crosses: single shart analyses from lowermost sample 30483. Triangles: single shart analyses from uppermost sample 22042. Diamonds: fused glass from 19337.

Fig. 6. Enlarged portion of the SiO_2-Al_2O_3-(Na_2O+K_2O) molecular diagram adopted from Bailey and Macdonald (1970). Diamond: 19337 glass. Filled circle: average shard composition. Open circle: low silica analysis from 19416. Filled square: whole rock pumice analysis (19396P) from Jørgensen (in press). Thick line E.I.: Easter Island trend from Bailey and Macdonald (1970). Crosses A,B,C represents quartz-feldspar minima from Carmichael and Mackenzie (1963).

Fig. 7. Part of the An-Ab-Or diagram with all feldspar analyses plotted. Crosses: all analyses from 19337. Open circles: all analyses from 22024. Inverted triangle: oscillatory zoned feldspar from 19342. Open standing triangle: resorbed feldspar from 19342. Filled standing triangle: strongly normal zoned feldspar from 19342. Diamonds: microcrysts from 19342, q designates feldspar in acid quench clot, and h feldspar in hybrid fiamme.

Fig. 8. Formula units Al (symbols) + Fe (arrow points) plotted against formula units Si. Diagonal line represents Si+Al=16. Symbols as in Fig. 7.

Fig. 9. Part of the pyroxene quadrilateral. Filled circles: cores. Open circles: rims. Filled triangle: zoned pyroxene. Squares: groundmass pyroxenes. R: pyroxene rod in feldspar xenocryst in hybrid fiamme. Crosses: microcrysts in hybrid fiamme. Diamonds: quench pyroxenes from acid clot.
At the bottom the olivines. Open squares: phenocryst. Filled squares: groundmass olivines.

Fig. 10. Part of the Na-(Fe^{2+}+Mn)-Mn triangle. Symbols as in Fig. 9.

Fig. 11. a + b Minor elements Mn, Na, Al and Ti in formula units plotted against formula units Mg. Symbols as in Fig. 9.

Fig. 12. Formula units Al versus Ti. The two diagonal lines represent Al:Ti 2:1 and 1:1. Symbols as in Fig. 9.

Fig. 13. Pyroxene quadrilateral for all acid pyroxenes. Hatched area: field of compositions from Fig. 9. Filled circles: zoned pyroxene from 22154. Open circles: resorbed pyroxene from 30483. Diamonds: quench clot pyroxenes from 19342.

Fig. 14. Oxide triangle after Carmichael (1967). Shaded area: field fo fayalite bearing rhyolites from Carmichael. Filled circles: the Thorsmörk ignimbrite oxides. Open circles: the Öræfajökull rhyolite from Carmichael (1967).

Fig. 15. Part of the minor element triangle for oxides after Carmichael (2967). Symbols as in Fig. 14. Heavy dashed lines are approximate trends for magnetites and ilmenites in Carmichael (1967).

Fig. 16. Groundmass feldspars from 19337 (open circles). Diamonds are phenocrysts from the same sample. Double circles are normative range of glass.

Fig. 17. fO_2-T diagram, with the range for the different samples shown (graphically determined values). The hatched circle shows the approximate position of the groundmass assemblage from 19337. Star indicates approximate position of hybrid fiamme from 19342 based on two geothermometers. Buffer curves adopted from Nicholls and Carmichael (1969).

Fig. 18. Comparison of Fe-Ti oxide temperatures with plagioclase temperatures for different samples. Diagonal line is the line of equal temperature.

Fig. 19. Crystallization diagram. See text for explanation.

Fig. 20. Variation of alkali ratio with Al_2O_3 (molecular), adopted from Bailey and Macdonald (1970). Symbols as in Fig. 6, with feldspar range for the Thorsmörk ignimbrite indicated on the feldspar line.

Fig. 21. Part of the normative Qz-Ab-Or diagram, modified from Wetzel et al. (1978). Symbols as in Fig. 6. Dotted line connecting crosses represents ternary minima in the system from .5 to 10 kb PH_2O. Tie lines connect least silicic compositions with range of feldspars from the Thorsmörk ignimbrite.

Fig. 22. Hypothetical N-S cross section of the crust beneath the Tindfjallajökull central volcano, showing position of magma chamber and possible level of partial melting. The boundaries 2-3 and 3-4 based on Palmason (1971). The intracaldera dome Ymir is postignimbritic in age.

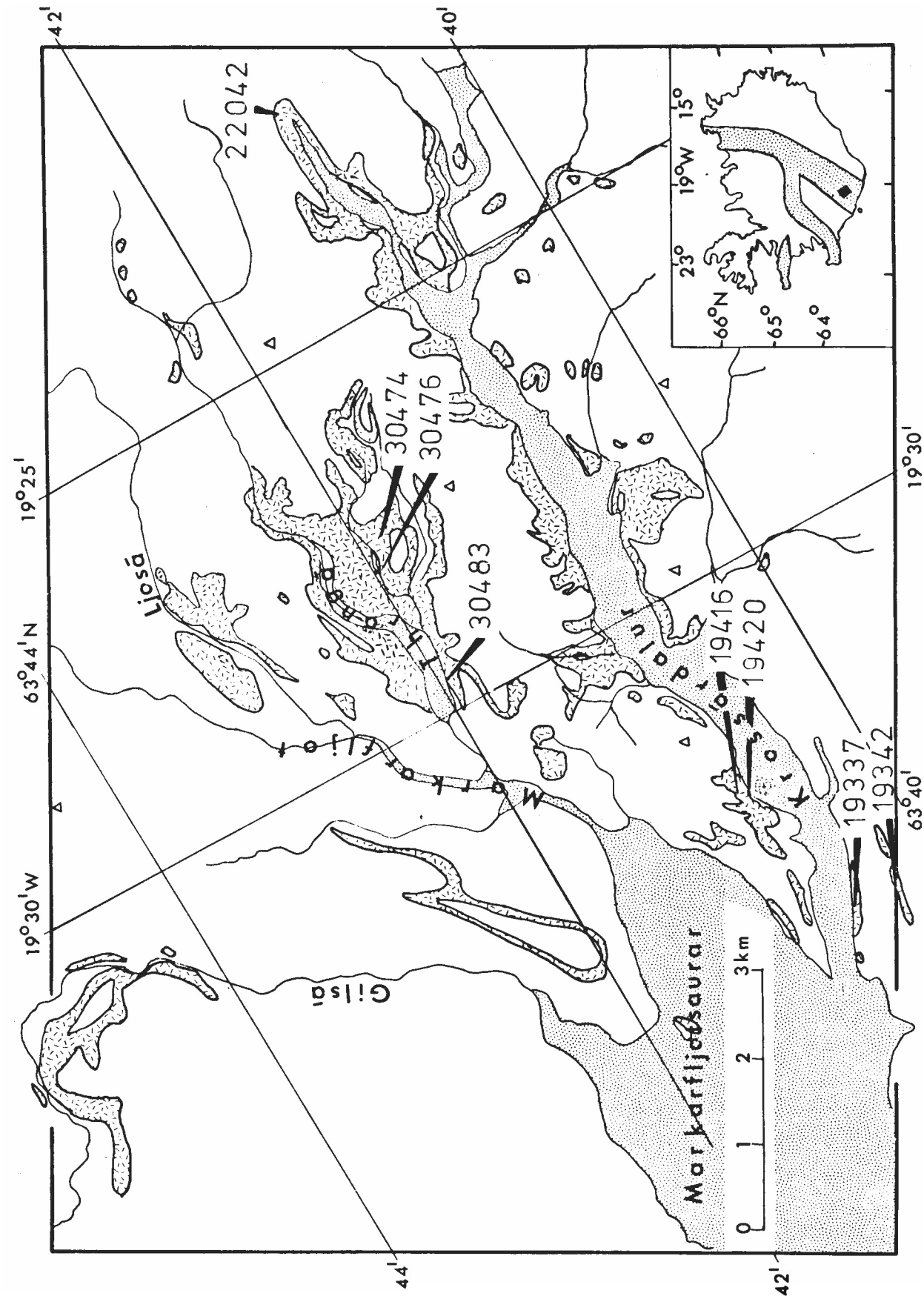
42'
40'
22042
30474
30476
30483
19416
19420
19337
19342
Ljosá
Gilsá
Marbarflijót
Saurar
19°25'
19°30'W
19°30'
63°44'N
63°40'
44'
42'
0
1
2
3km
15°
19°W
23°
66°N
65°
64°

Fig. 1

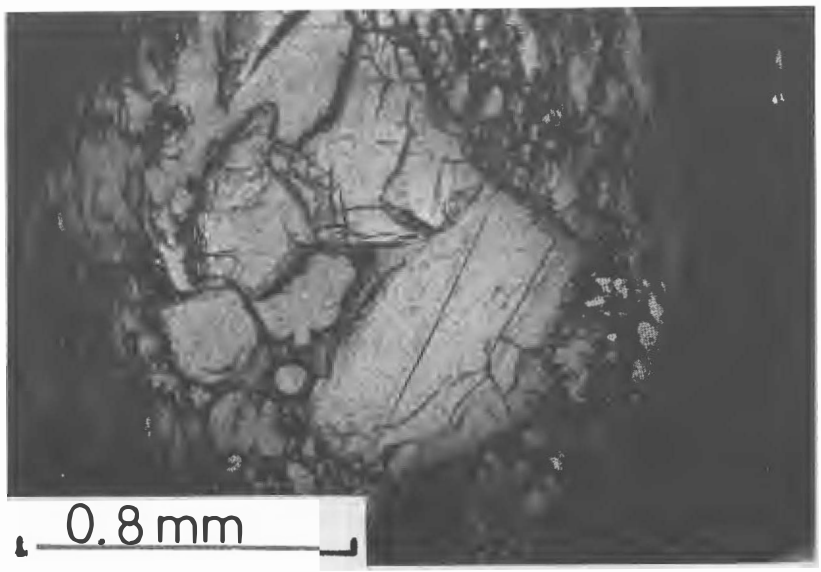

Fig. 2

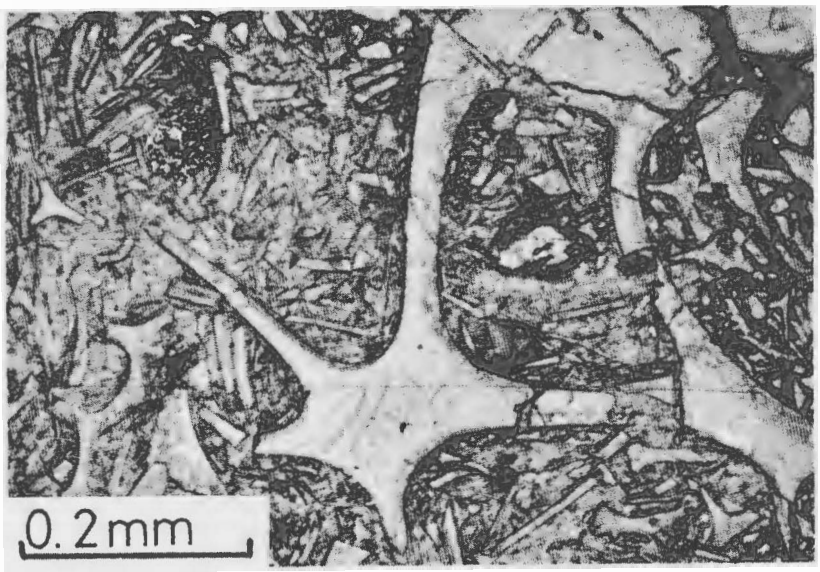

Fig. 3

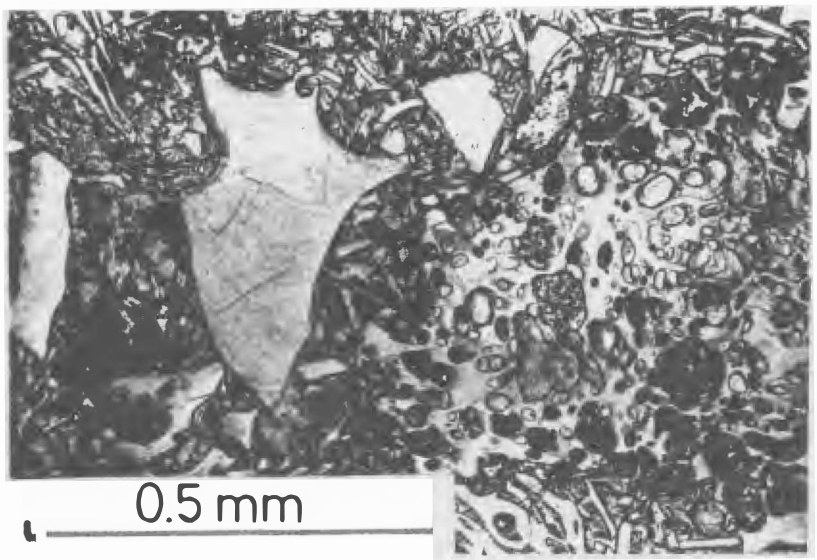

Fig. 4

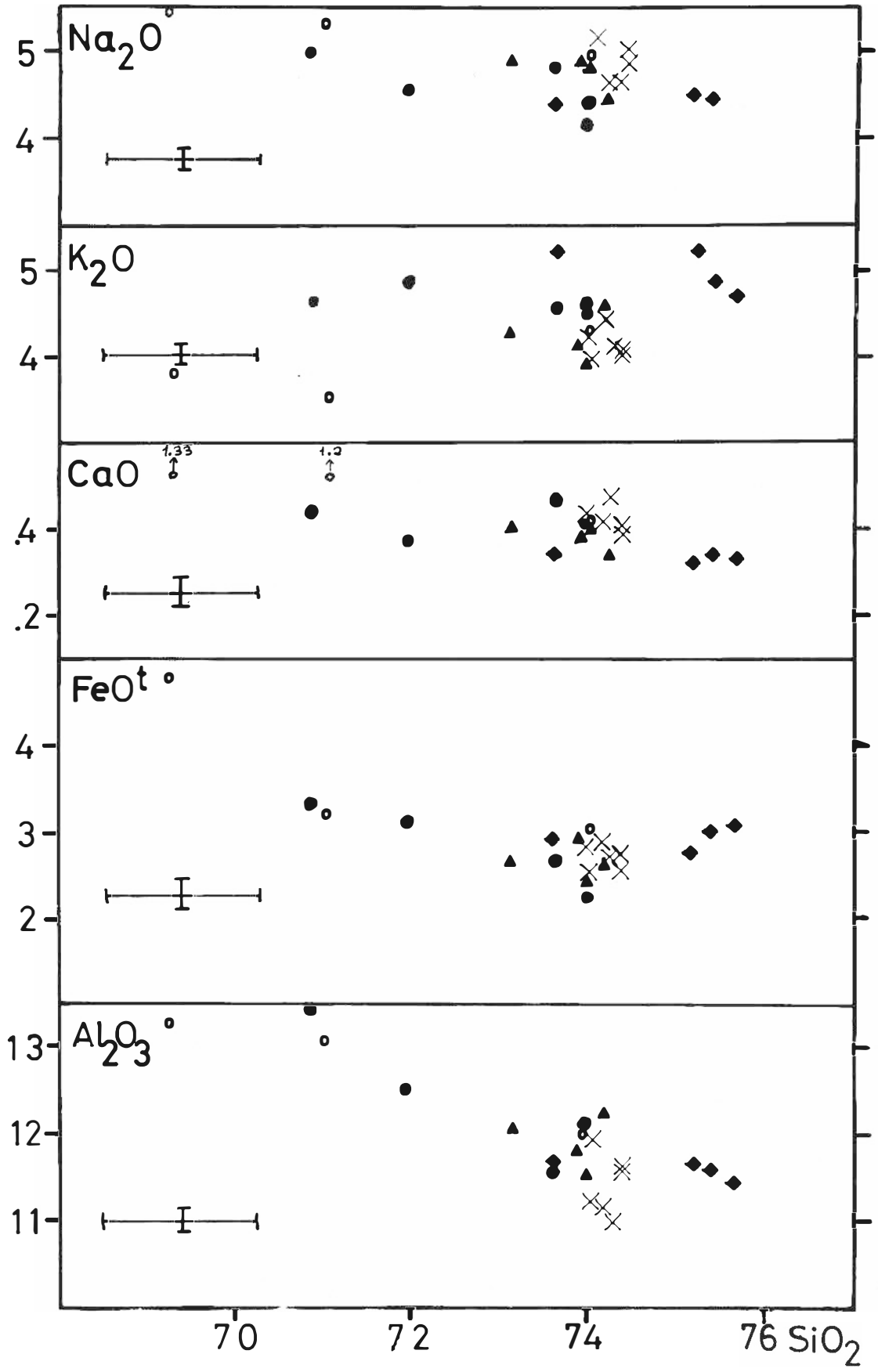
Na2O
5
4
K2O
5
4
1.33
1.2
CaO
.4
.2
FeOt °
4
3
2
Al2O3 °
13
12
11
70
72
74
76 SiO2

Fig. 5

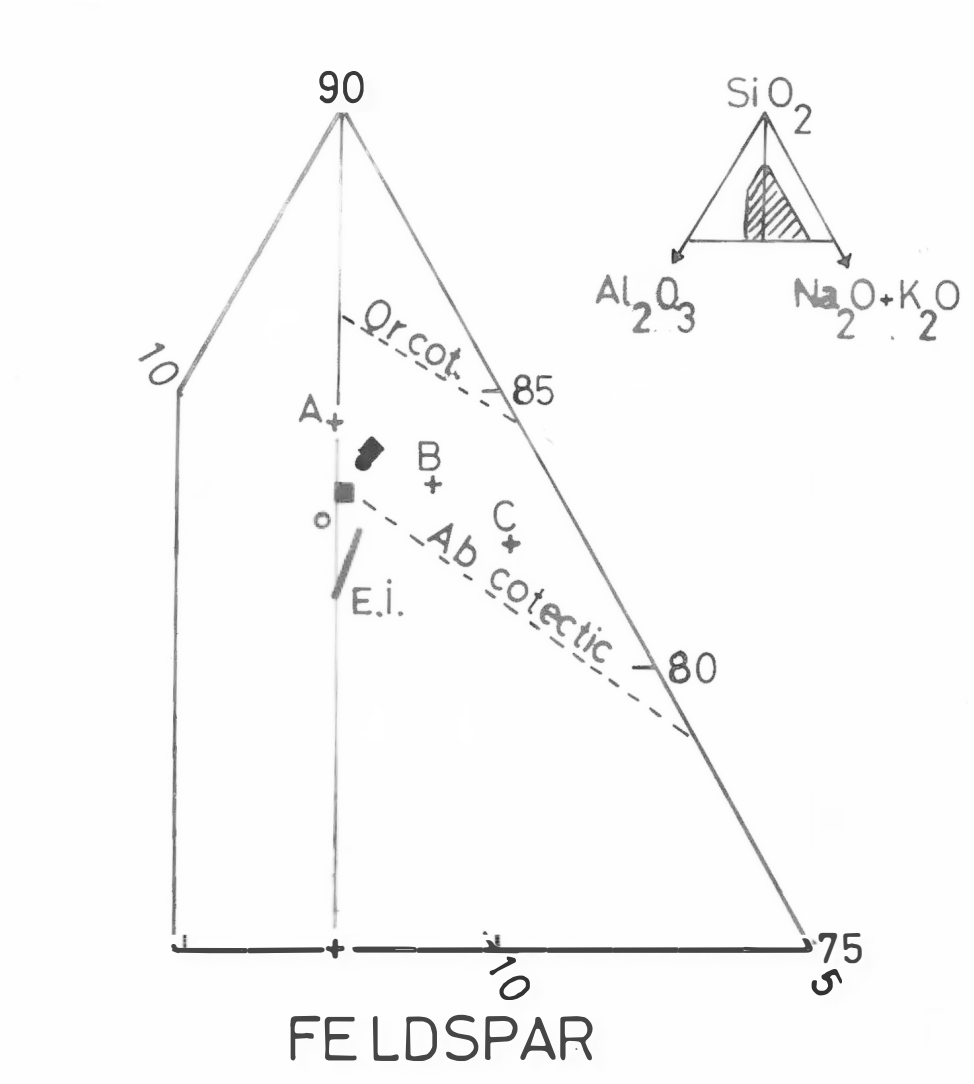
90
SiO2
Al2O3
Na2O+K2O
Qr cot.
85
10
A
B
C
Ab cotectic
80
E.i.
75
10
5
FELDSPAR

Fig. 6

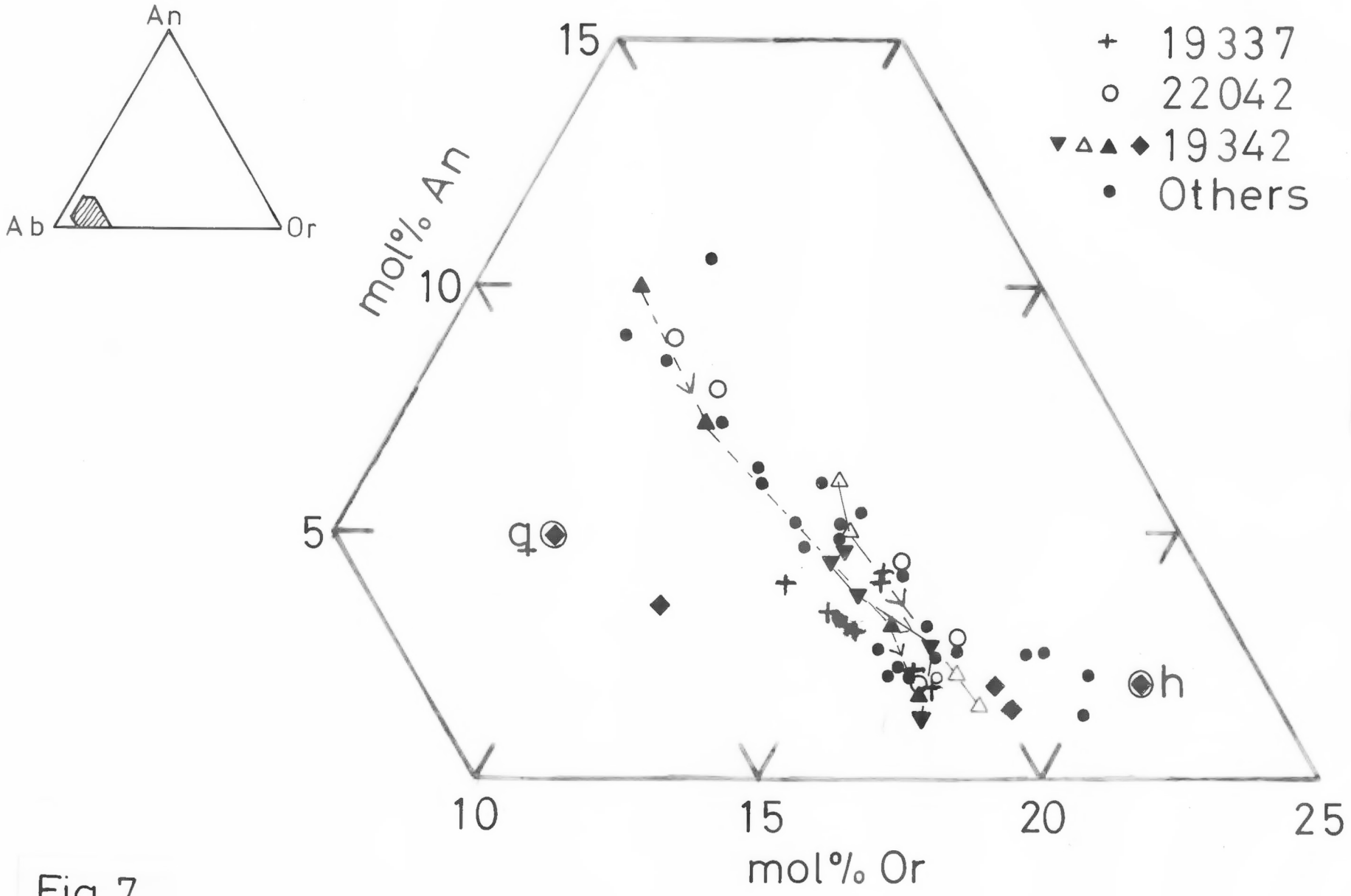
An
Ab
Or
15
10
5
mol% An
10
15
20
25
mol% Or
+ 19337
o 22042
▼△▲◆ 19342
• Others
q
h

Fig. 7

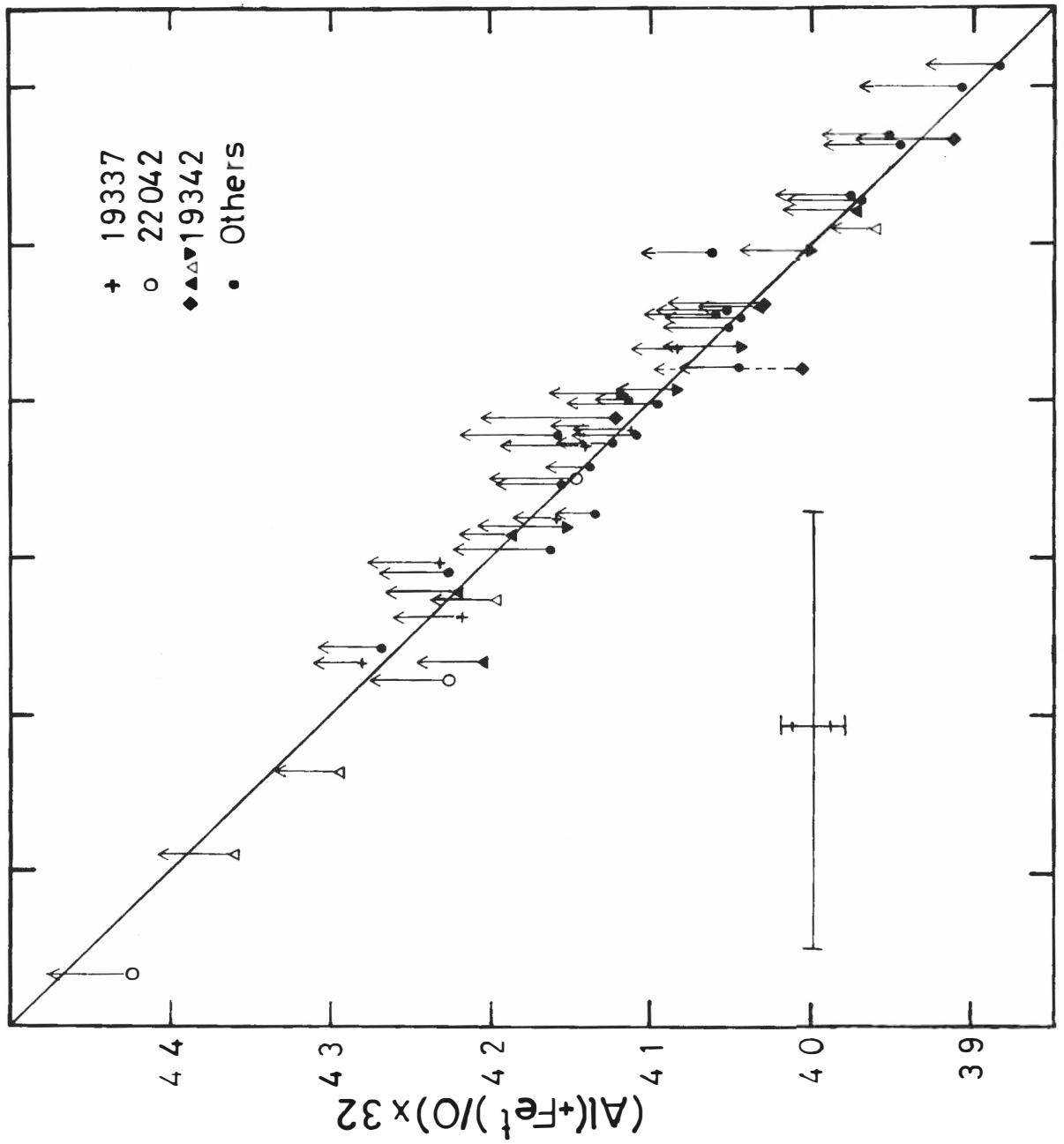
+ 19337
○ 22042
◆▲△▼19342
• Others
(Al(+Fe^t)/O)x 32
(Si/O)x32
4.4
4.3
4.2
4.1
4.0
3.9
11.6
11.7
11.8
11.9
12.0
12.1

Fig 8

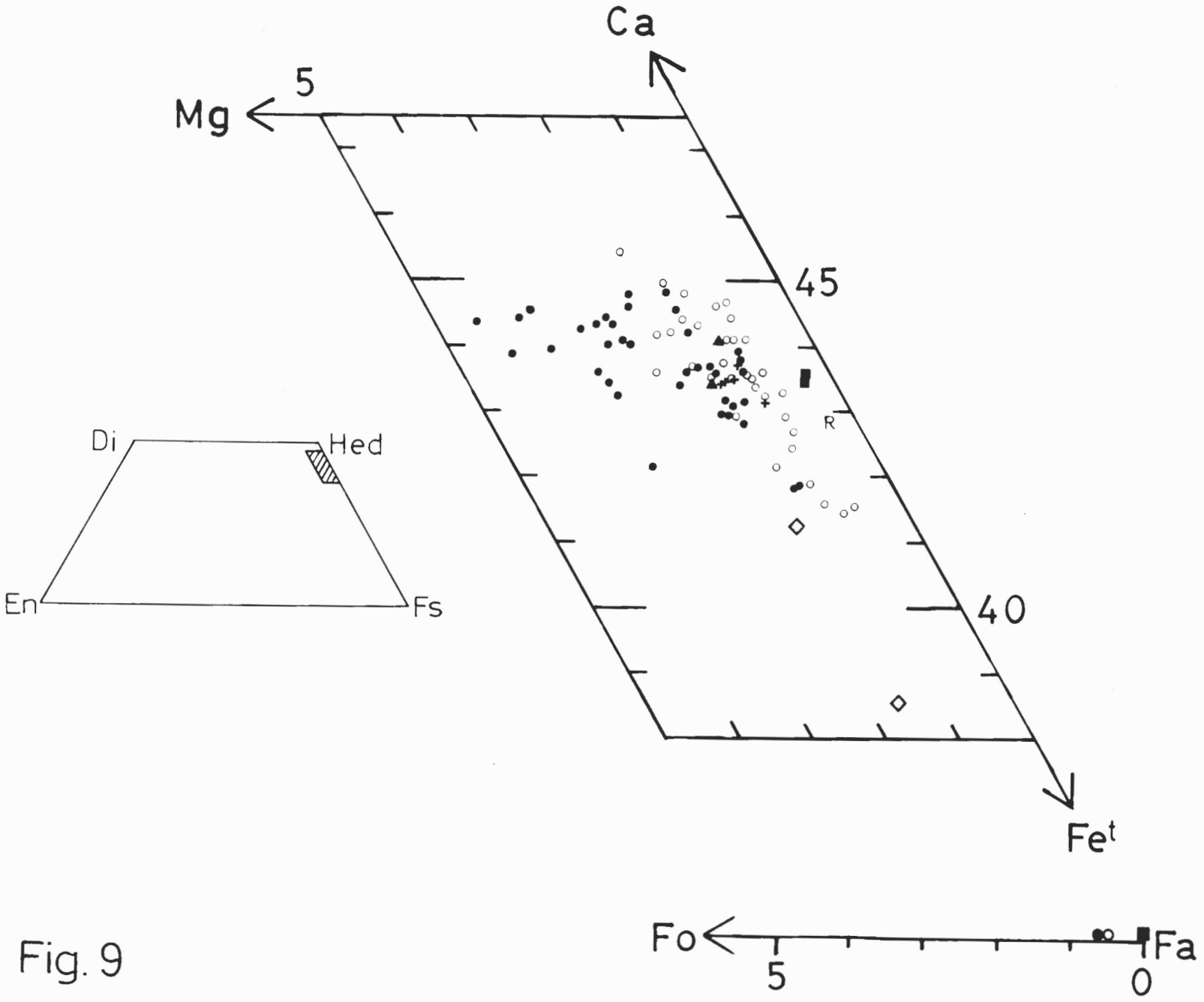

Fig. 9

Fig. 10

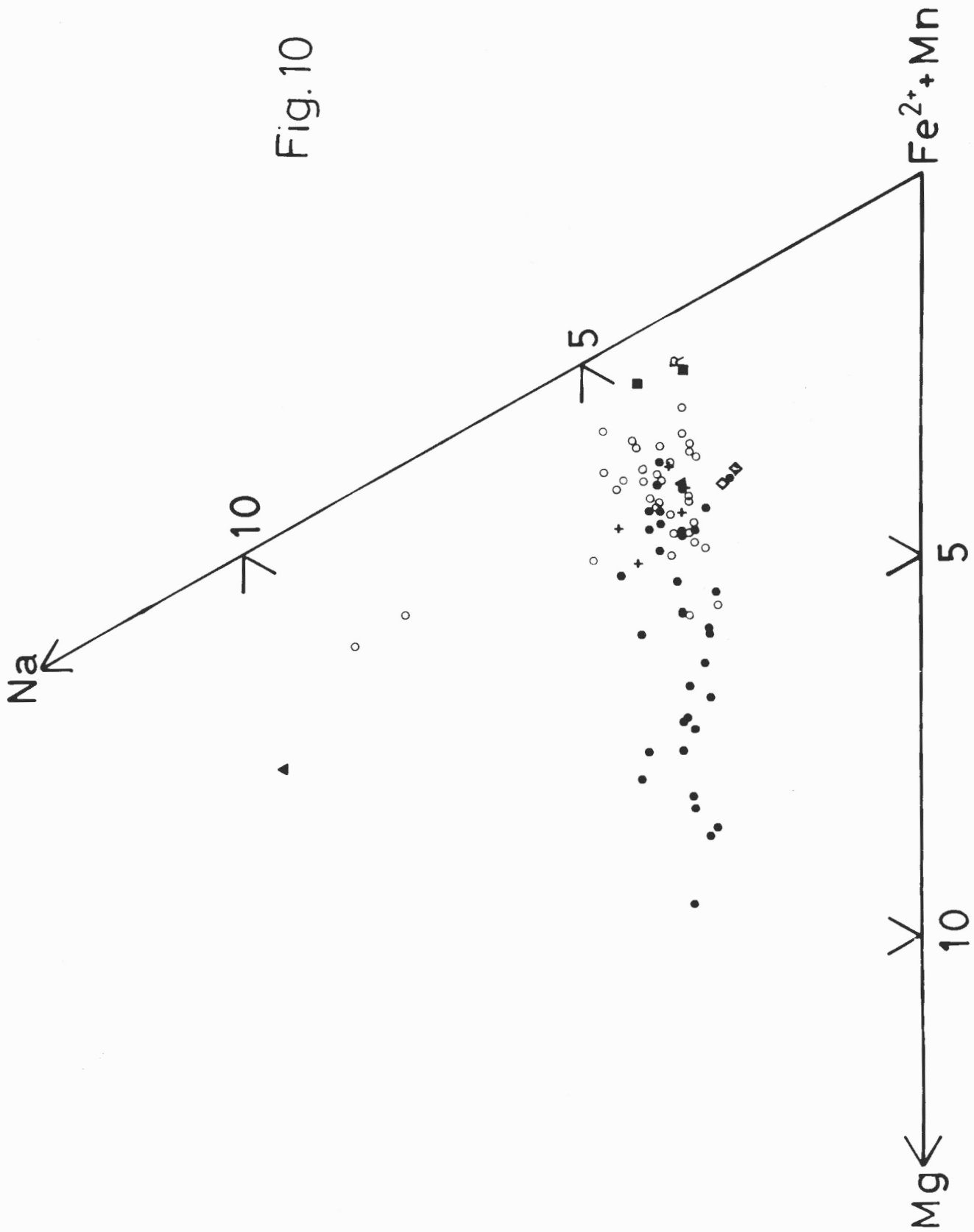

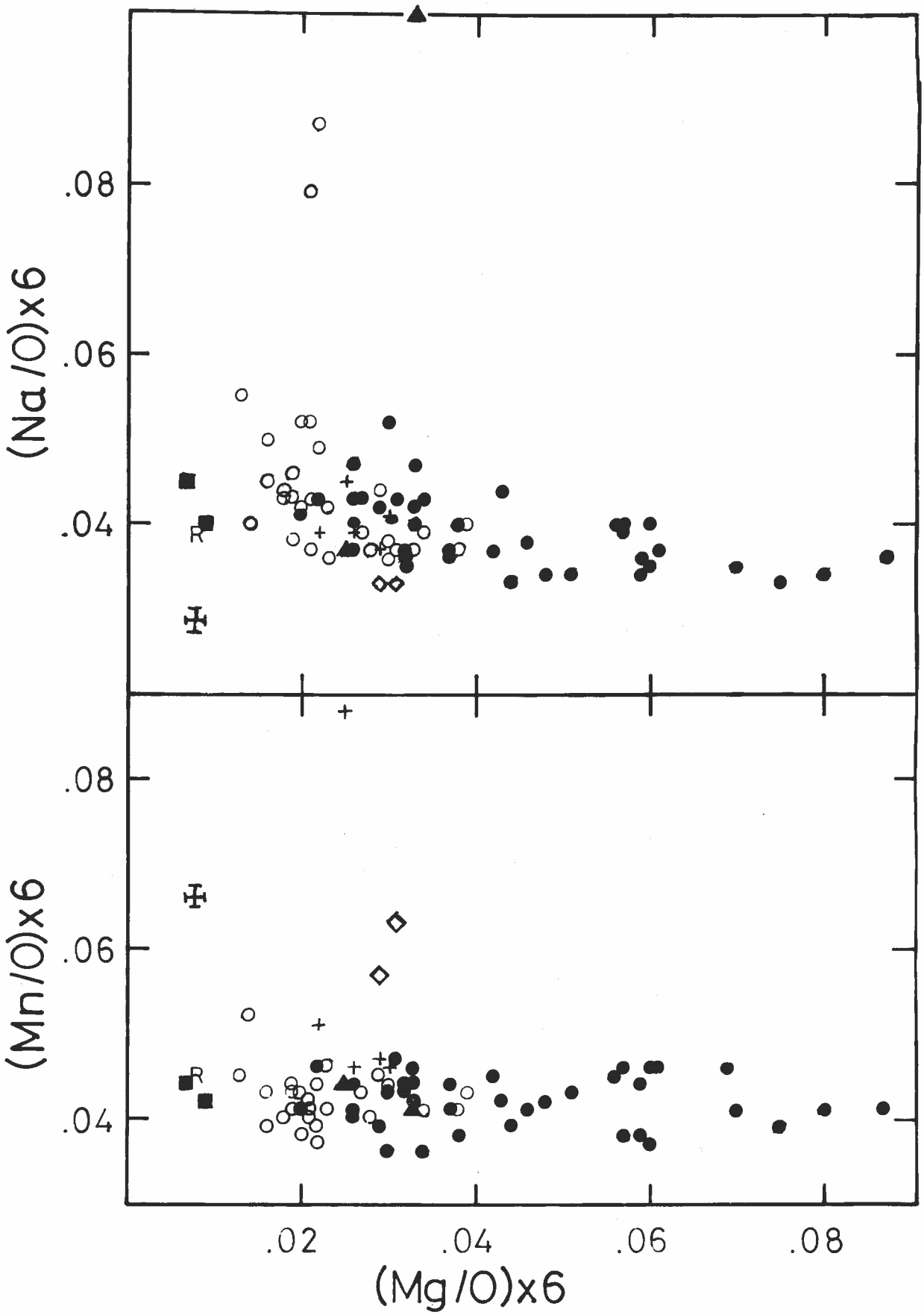

Fig. 11a

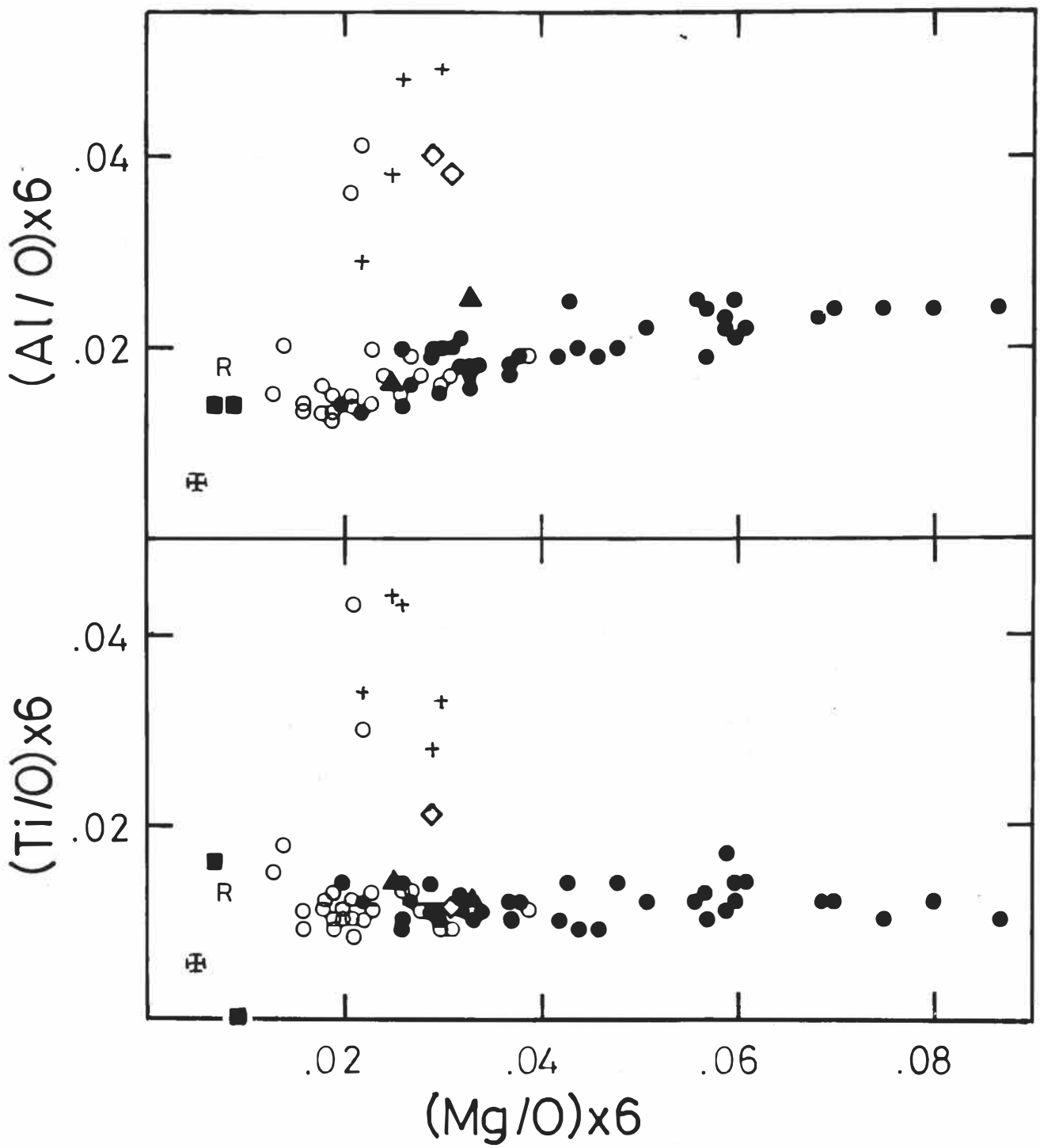

Fig. 11b

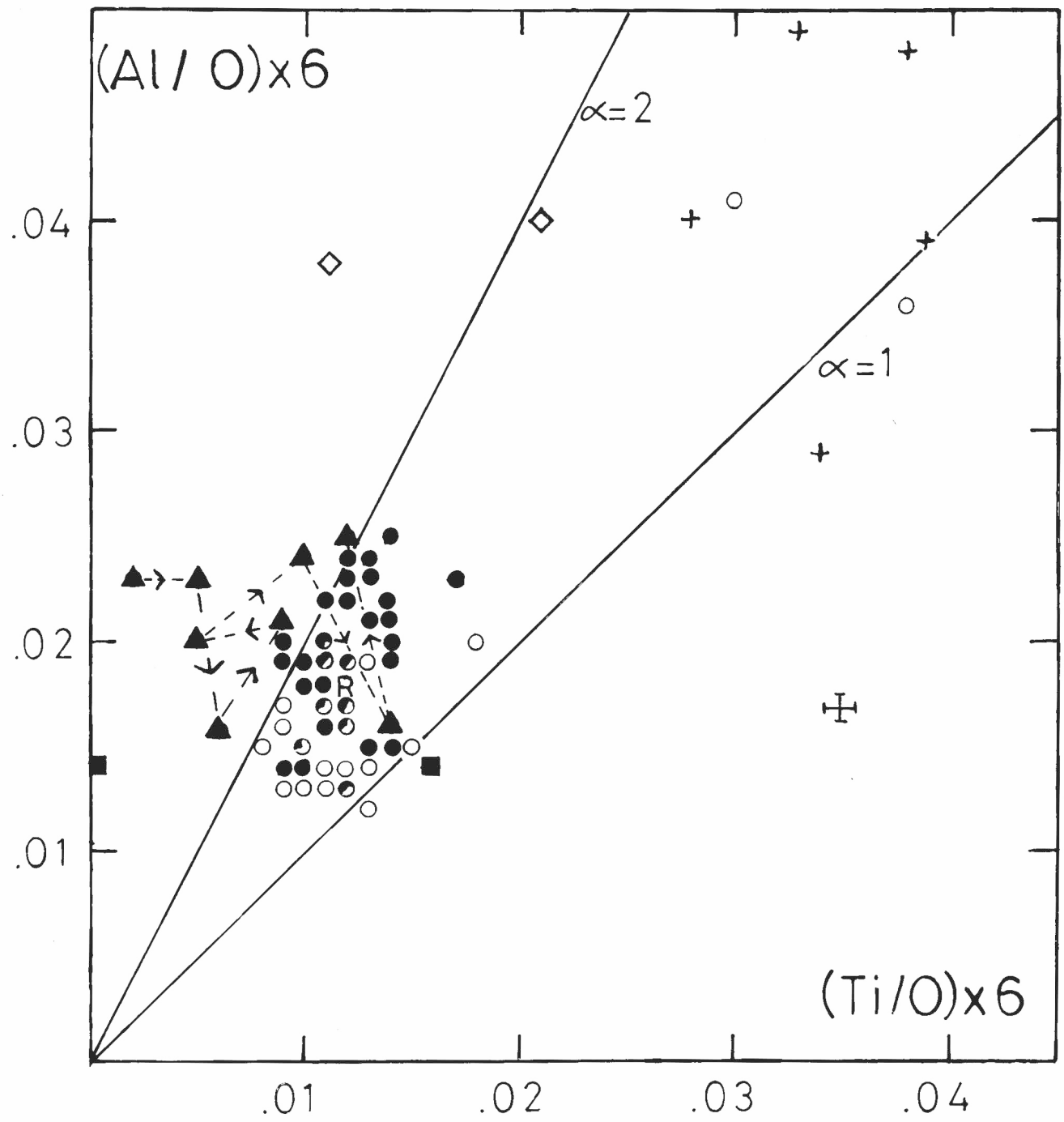

Fig. 12

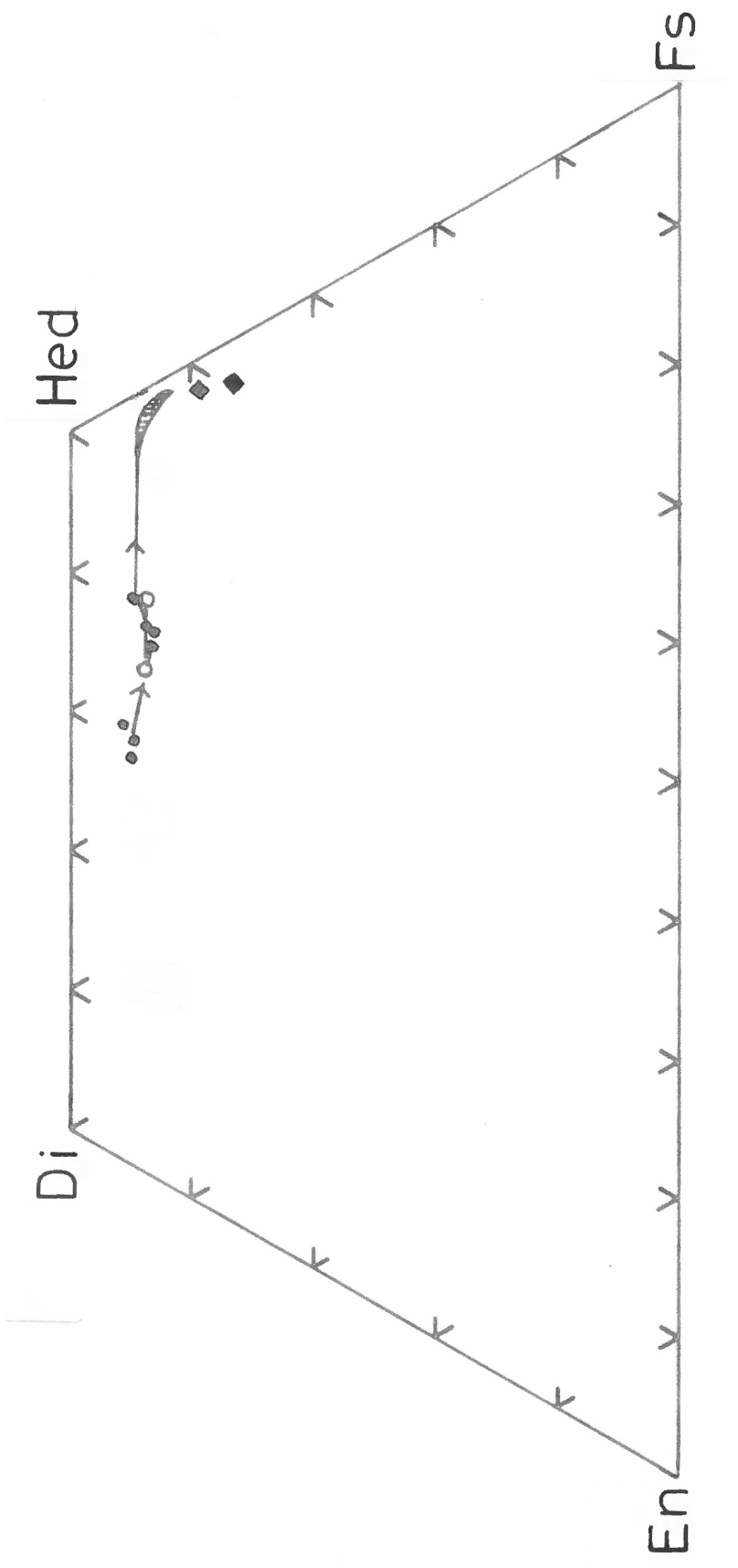

Fig. 13

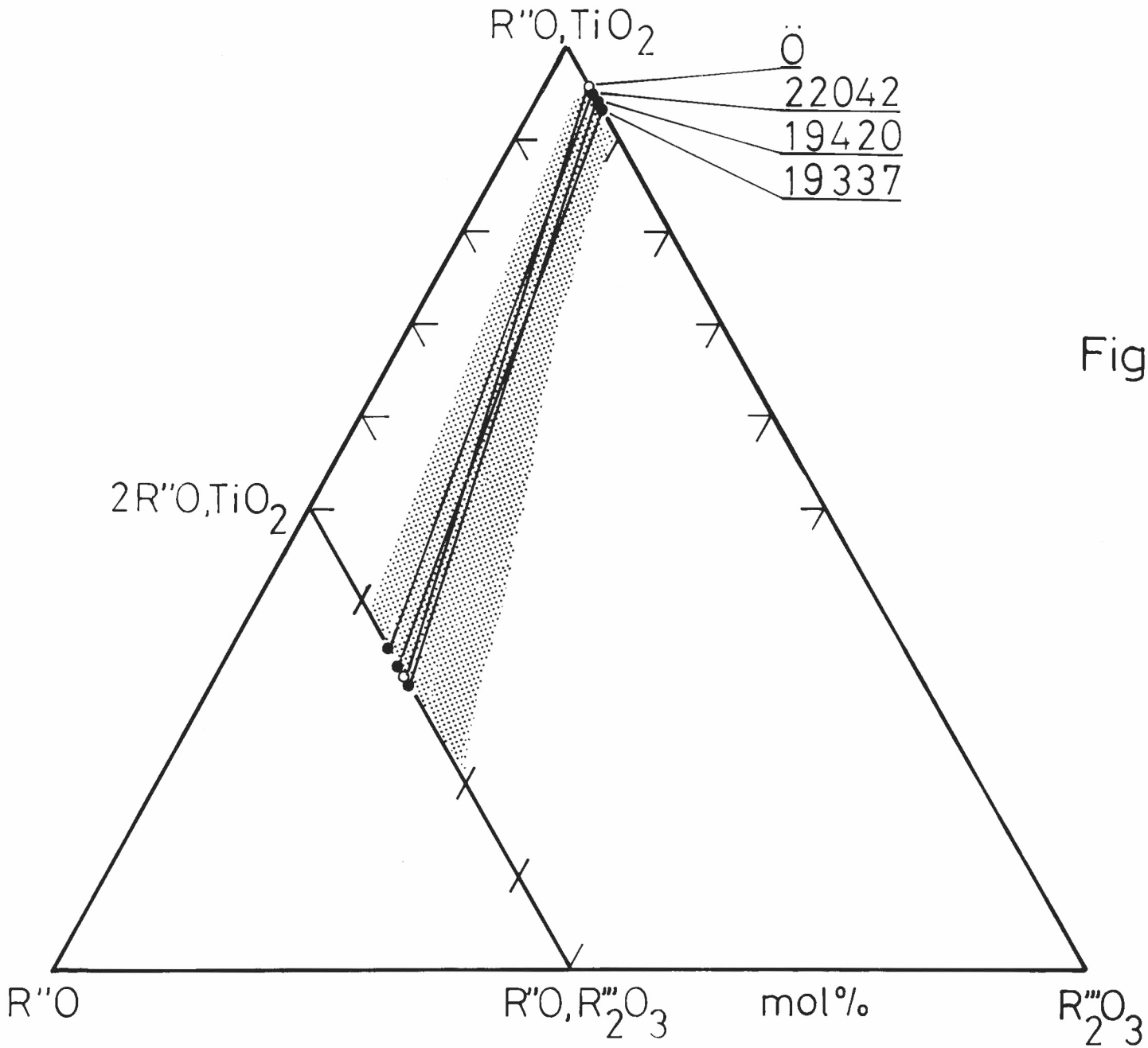

Fig. 14

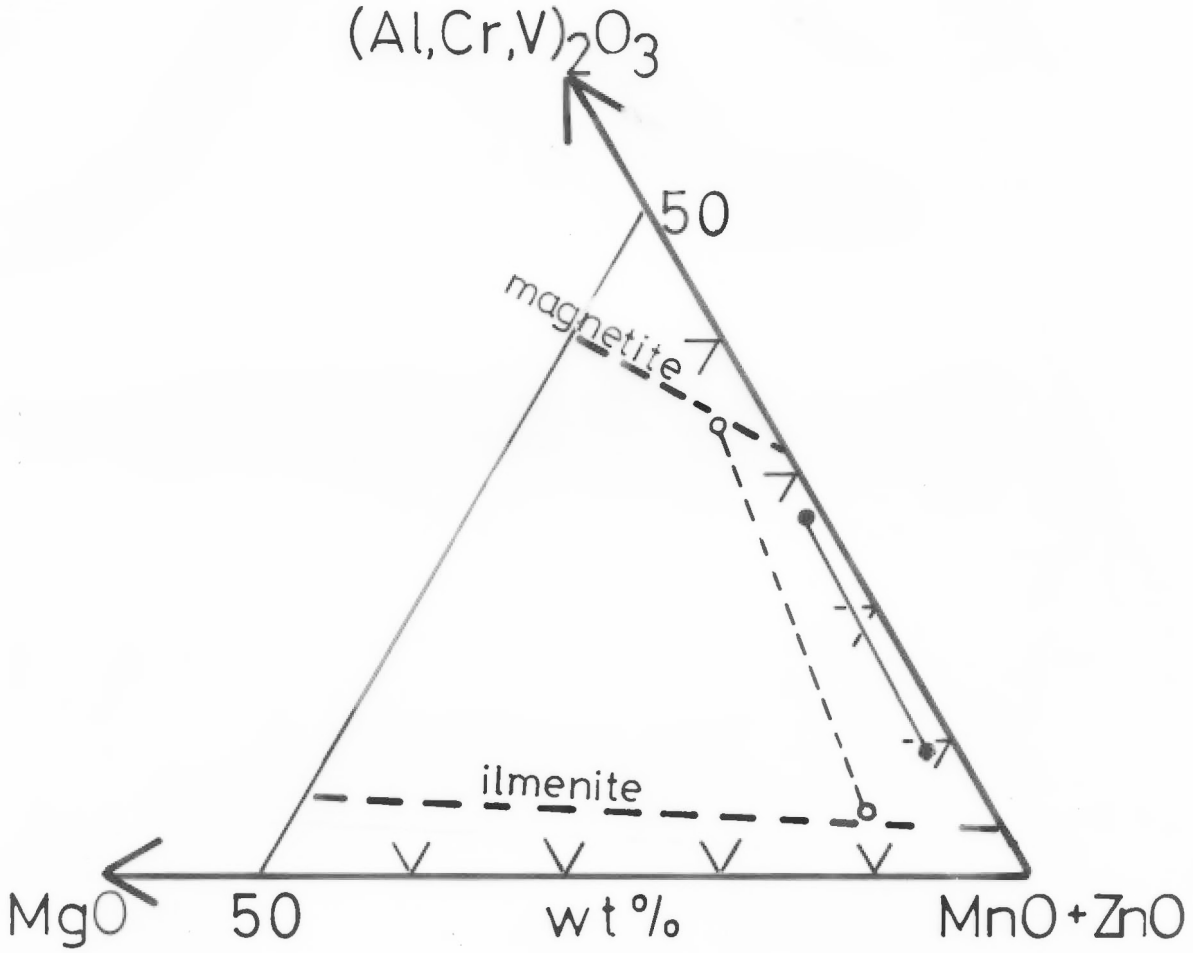

Fig. 15

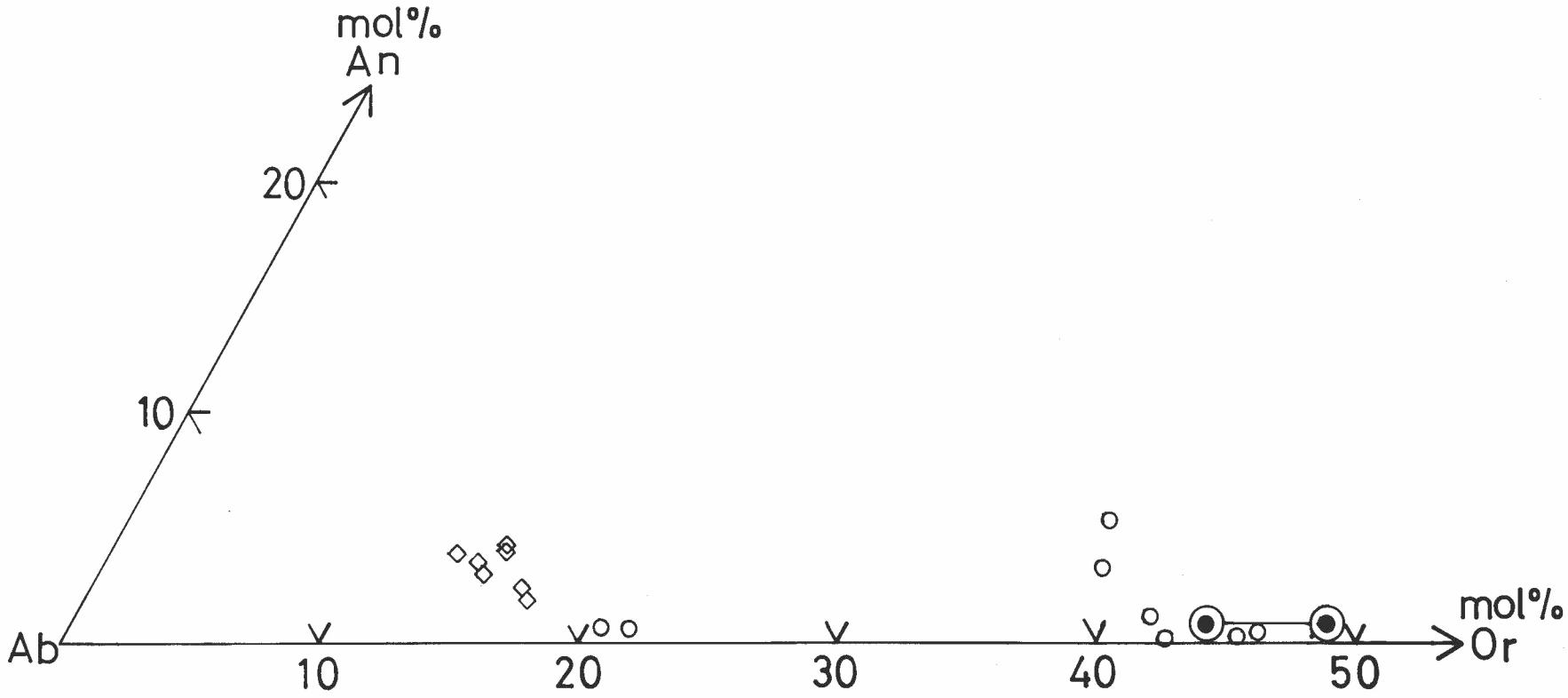

Fig. 16

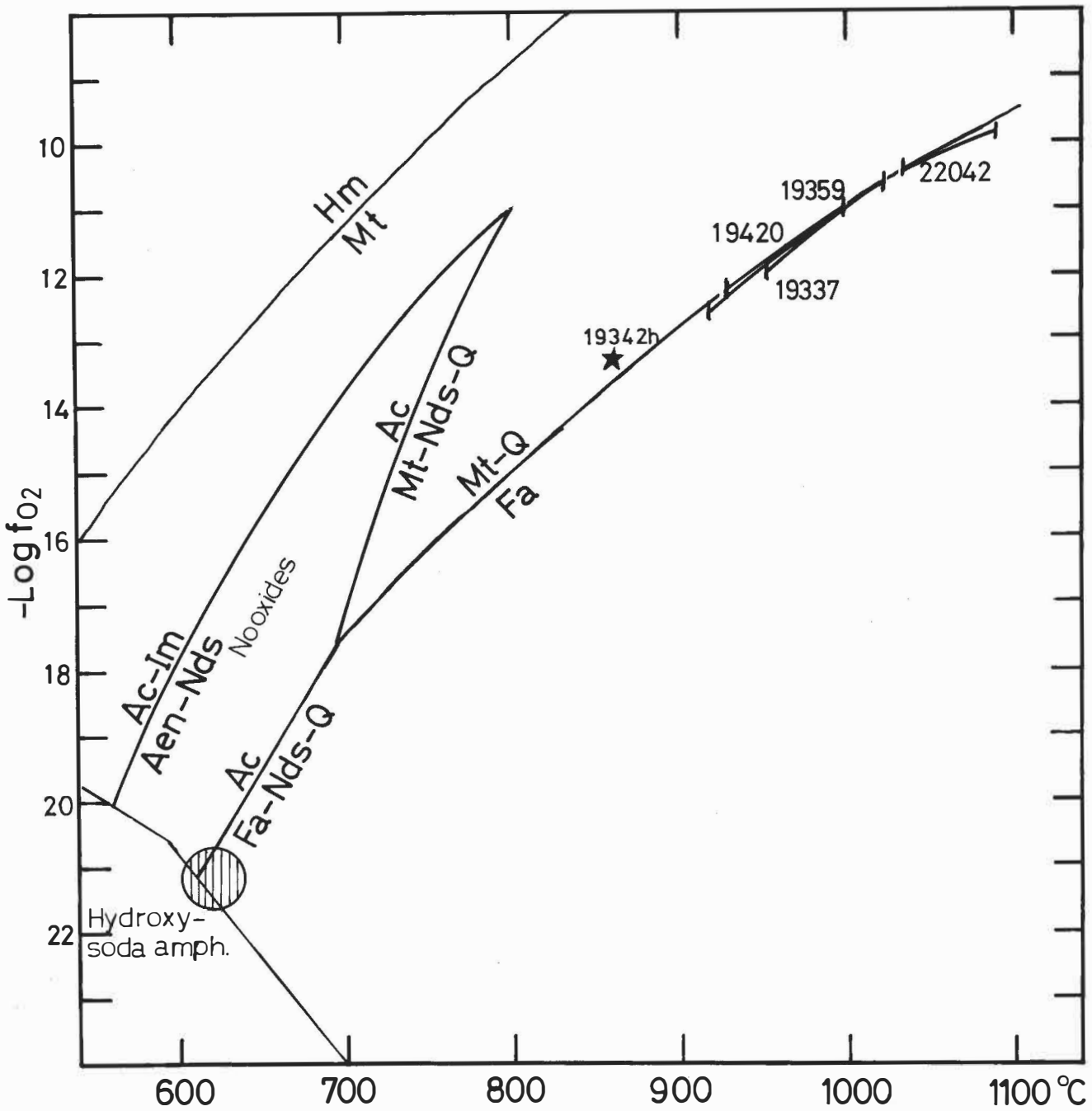
-Log f_{O_2}
10
12
14
16
18
20
22
600
700
800
900
1000
1100 °C
Hm
Mt
Ac
Mt-Nds-Q
Mt-Q
Fa
Ac-Im
Aen-Nds
No oxides
Ac
Fa-Nds-Q
Hydroxy-
soda amph.
19359
22042
19420
19337
19342h

Fig.17

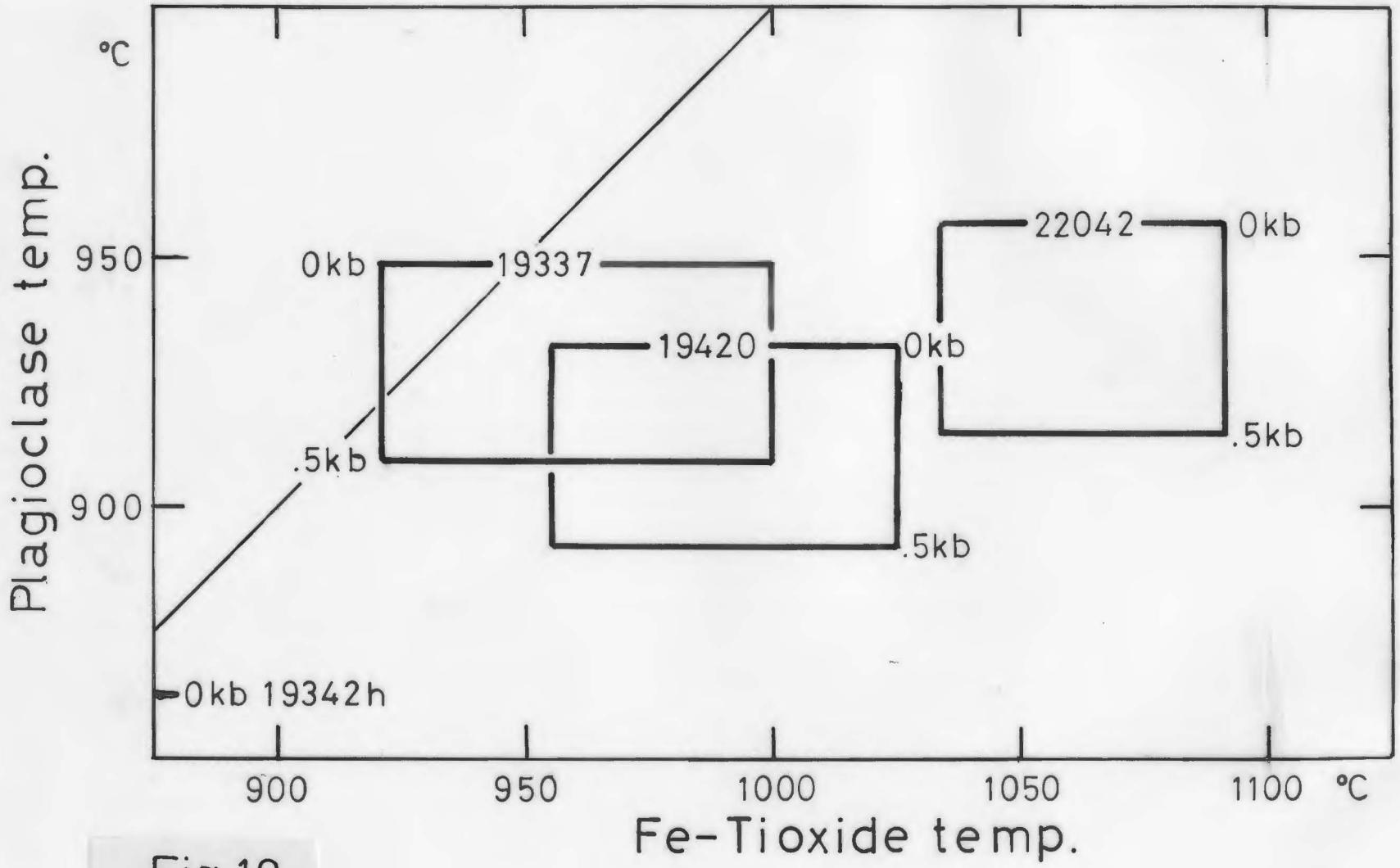
Plagioclase temp.
℃
950
900
0kb
19337
.5kb
19420
0kb
.5kb
22042
0kb
.5kb
0kb 19342h
900
950
1000
1050
1100
℃
Fe-Tioxide temp.

Fig.18

Crystallization Diagram

Feldspar	large An_9	normal An_5	micro An_2
Pyroxene	large $En_{3.8}$ (Ca-Ti-Tsch)	normal $En_{2.6}$	micro En_1 (NAT)
Fayalite			$Fo_{.5}$ $Fo_{.4}$
Magnetite			exs.
Ilmenite			
Zircon			
Chevkinite			
Apatite			
Crystallinity in est. vol.%	1	6	10

Fig. 19

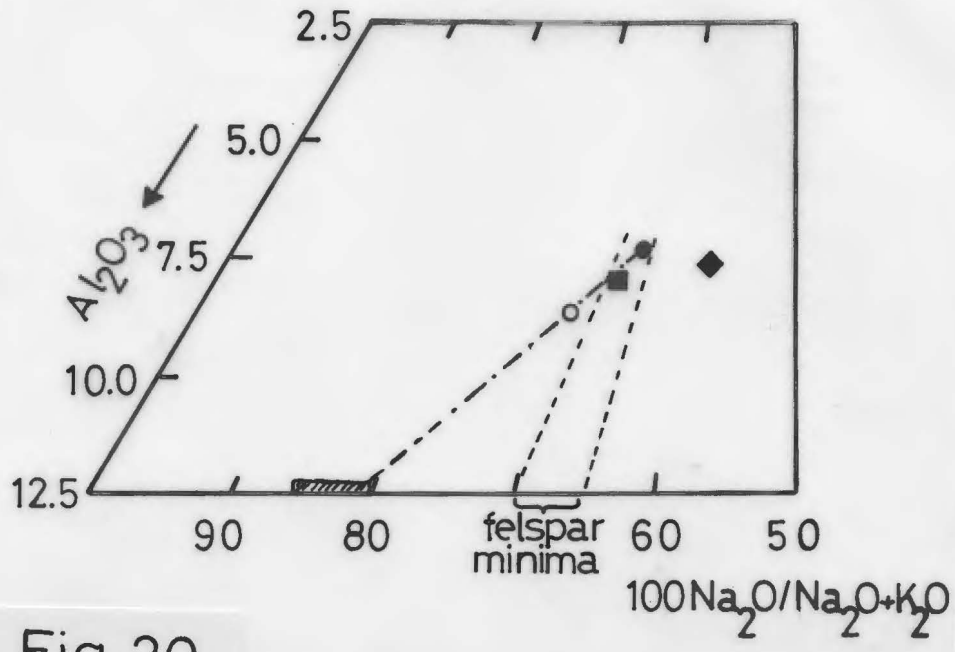
2.5
5.0
7.5
10.0
12.5
Al_2O_3
90
80
felspar
minima
60
50
$100Na_2O/Na_2O+K_2O$

Fig. 20

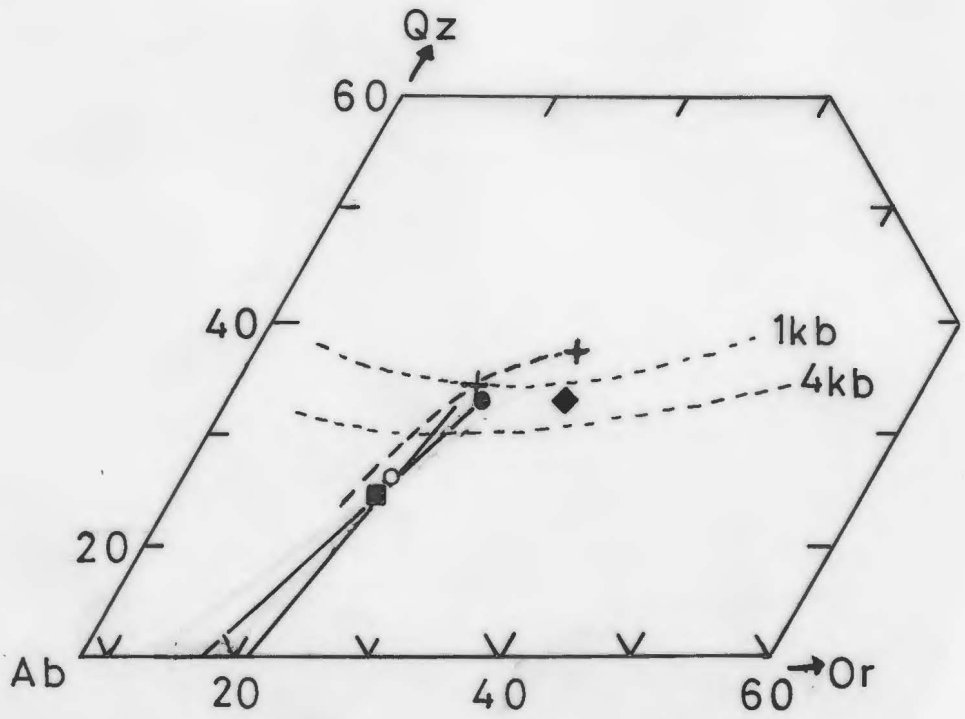
Qz
60
40
20
Ab
20
40
60
Or
1kb
4kb

Fig. 21

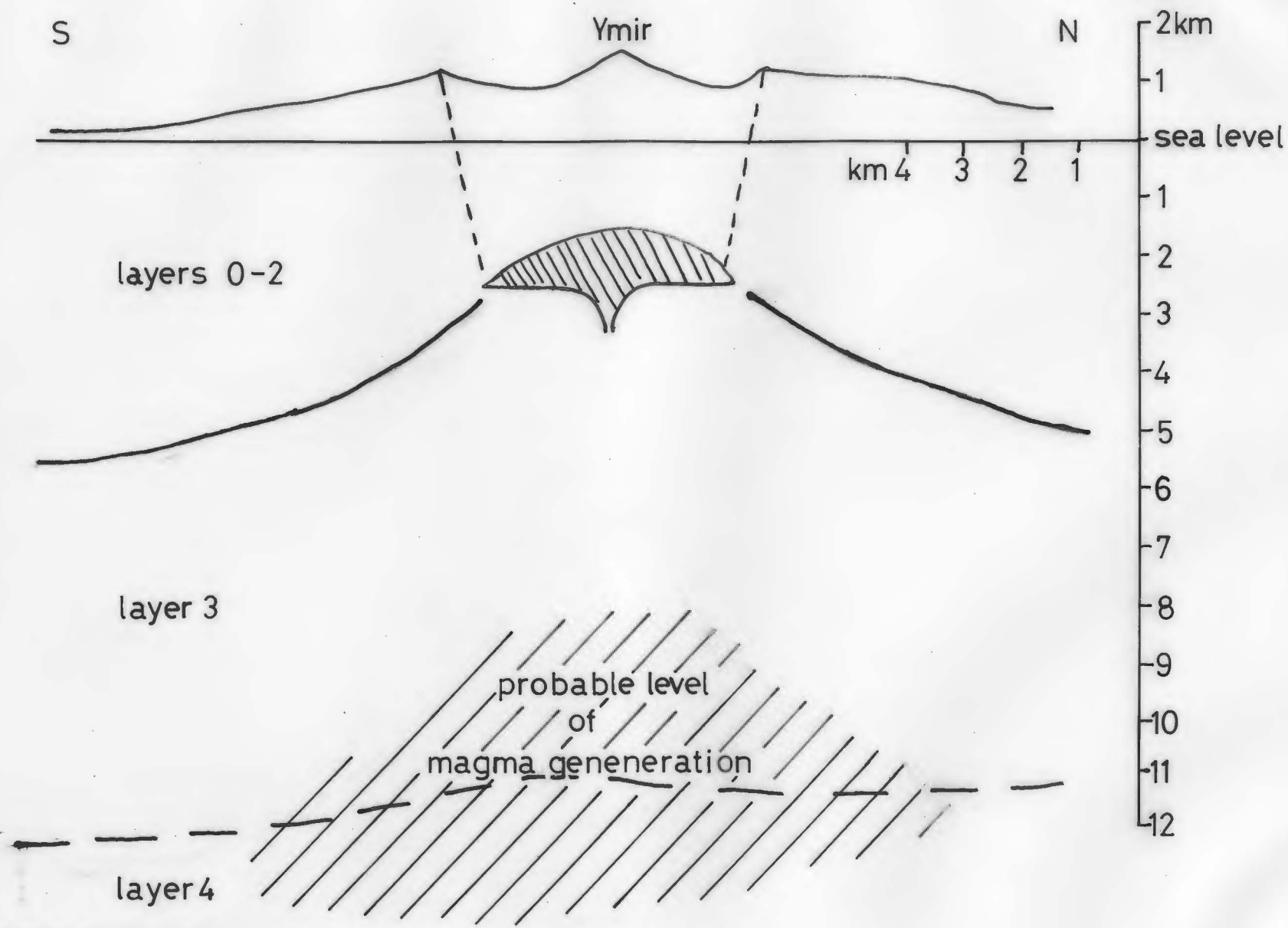
S
Ymir
N
2km
1
sea level
km 4 3 2 1
1
2
3
4
5
6
7
8
9
10
11
12
layers 0-2
layer 3
probable level
of
magma genegeneration
layer 4

Fig. 22

Appendix 1 Feldspar analyses

sample	type	SiO_2	Al_2O_3	FeO^t	CaO	Na_2O	K_2O	Sum	An	Ab	Or
19342	c	68.65	20.14	.14	1.05	9.21	2.40	101.59	5.1	81	13.9
	r	68.16	20.20	.20	1.20	9.29	2.31	101.36	5.8	81	13.2
	c	68.24	20.16	.17	1.02	9.31	2.19	101.10	5	82.3	12.7
	c	68.96	20.24	.27	1.06	9.51	2.36	102.40	5	81.7	13.3
	c	66.84	20.33	.28	1.03	9.29	2.30	100.07	5	81.7	13.3
	r	68.49	19.65	.31	.49	9.31	2.88	101.13	2.4	81.1	16.5
	c	69.09	19.86	.33	.92	9.45	2.48	102.12	4.4	81.5	14.1
	c	67.61	20.15	.36	.99	9.52	2.55	101.17	4.7	81.1	14.3
	b	68.64	19.98	.25	.77	9.43	2.65	101.71	3.7	81.3	15
	r	69.11	19.98	.29	.53	9.17	2.91	101.57	2.6	80.6	16.8
	r	67.03	19.67	.31	.25	9.23	2.99	99.49	1.2	81.4	17.3
	c	68.81	20.92	.28	2.15	9.90	1.47	103.52	9.8	82.1	8
	c	67.82	20.63	.30	1.48	9.47	1.83	101.53	7.1	82.4	10.5
	r	69.27	19.83	.28	.63	9.36	2.78	102.14	3	81.1	15.8
	r	69.75	19.54	.33	.33	9.38	2.98	102.31	1.6	81.4	17
	c	69.66	20.55	.24	1.16	9.46	2.34	103.41	5.5	81.3	13.2
	r	68.55	19.75	.30	.54	9.20	2.71	101.06	2.6	81.6	15.8
	m	68.76	19.66	.42	.43	9.35	2.83	101.46	2.1	81.6	16.3
	m	67.67	19.30	.63	.70	9.95	2.06	100.30	3.3	85.1	11.6
	m	70.00	19.25	.42	.30	9.11	3.27	102.34	1.4	79.7	18.8
	m	66.48	19.58	.56	.39	8.90	3.08	98.10	1.9	79.9	18.2
	mh	67.58	17.71	.90	.32	7.70	3.12	97.45	1.8	77.5	20.7
	q	68.14	18.57	.77	.93	9.27	1.46	99.23	4.8	86.3	9
19337	c	67.90	19.94	.26	.71	9.51	2.57	100.90	3.4	82	14.6
	c	67.01	20.03	.18	.66	9.63	2.69	100.20	3.1	81.9	15
	r	67.31	19.92	.37	.45	9.23	2.91	100.19	2.2	81	16.8
	c	66.42	20.22	.30	.83	9.07	2.60	99.44	4.1	80.7	15.2
	c	66.39	20.20	.28	.84	9.54	2.73	99.99	4	80.8	15.2
	r	68.23	19.80	.19	.36	9.30	2.99	100.87	1.8	81.1	17.2
	c	65.73	20.35	.22	.82	9.56	2.37	99.04	3.9	82.6	13.5
	r	67.28	20.02	.26	.62	9.49	2.66	100.34	3	81.9	15.1
30483	c	69.86	19.57	.31	.53	8.92	3.24	102.44	2.6	78.6	18.8
	c	70.41	20.57	.36	1.48	9.37	1.86	104.06	7.2	82.1	10.7
	c	68.76	21.21	.27	2.23	9.07	1.49	103.04	10.9	80.4	8.7
	r	70.25	19.26	.42	.26	8.70	3.38	102.26	1.3	78.6	20.1
	c	68.49	20.35	.38	1.19	8.97	2.01	101.38	6	81.9	12.1
	r	67.84	20.29	.41	1.12	9.41	2.53	101.59	5.3	80.5	14.2
	c	70.47	19.56	.32	.53	8.95	2.93	102.75	2.6	80.1	17.3
	r	68.37	19.66	.30	.54	8.88	3.20	100.94	2.6	80.1	18.7

Appendix 1 Feldspar analyses continued

sample	type	SiO_2	Al_2O_3	FeO^t	CaO	Na_2O	K_2O	Sum	An	Ab	Or
30483	c	66.44	10.24	.13	.67	9.30	2.54	89.32	3.3	82	14.7
	r	70.07	19.47	.28	.45	9.02	2.76	102.05	2.3	81.4	16.4
	c	69.11	19.84	.27	.68	8.89	2.88	101.68	3.4	79.6	17
	r	68.88	19.58	.32	.40	9.02	2.91	101.12	2	80.8	17.2
	c	70.62	20.29	.29	.82	8.77	2.58	103.38	4.2	80.3	15.5
	r	66.71	19.68	.32	.64	9.07	2.83	99.25	3.1	80.4	16.5
	r	70.10	19.66	.34	.51	8.90	3.17	102.67	2.5	78.9	18.5
	r	70.48	19.16	.30	.41	9.06	2.91	102.31	2	80.9	17.1
	r	67.27	18.54	.21	.39	8.26	3.19	97.85	2.1	78.1	19.8
19420	r	60.05	20.14	.12	1.31	9.36	2.07	93.05	6.3	81.8	11.9
	c	64.94	20.81	.00	1.78	9.54	1.59	98.66	8.5	82.4	9.1
	c	63.46	20.81	.29	1.91	9.74	1.45	97.67	9	82.9	8.1
	c	67.04	19.89	.16	1.01	9.67	2.42	100.19	4.7	81.8	13.5
	r	63.91	19.21	.21	.41	9.14	2.87	95.75	2	81.2	16.8
	c	65.01	19.67	.28	1.26	9.16	2.29	97.68	6.1	80.6	13.3
	r	60.13	18.80	.21	.42	9.14	3.15	91.85	2	79.8	18.1
	r	67.40	18.88	.19	.54	9.01	3.01	99.03	2.6	79.8	17.5
	r	62.17	19.82	.28	1.07	9.30	2.47	95.11	5.1	80.7	14.1
22042	c	68.15	20.22	.31	.91	9.19	2.71	101.50	4.4	80.1	15.5
	r	62.88	20.48	.32	1.86	9.50	1.61	96.65	8.9	82	9.1
	c	66.09	20.19	.32	1.66	9.53	1.85	99.56	7.9	81.7	10.4
	r	66.81	19.24	.25	.56	9.28	3.02	99.16	2.7	80.2	17.2
19337	Groundmass feldspars										
	g	63.56	16.14	2.07	1.01	5.72	6.85	95.34	5.2	53	41.8
	g	57.24	13.04	1.64	.00	4.90	5.63	82.46	0	56.9	43.1
	g	65.13	14.52	1.70	.54	5.34	5.90	93.13	3.1	56.1	40.8
	g	67.68	12.21	1.80	.06	4.14	5.29	91.17	.4	54.1	45.5
	g	68.98	14.70	1.54	.18	5.38	6.41	97.20	1	55.4	43.5
	g	67.62	13.75	1.75	.09	6.75	2.75	92.70	.5	78.4	21
	g	73.97	13.37	1.20	.06	6.69	2.85	98.14	.4	77.8	21.8

type explanation: c, core. r, rim. m, microcryst. mh, microcryst in hybrid fiamme. q, feldspar from acid quench clot. b, band in feldspar between core and rim. g, grounmass feldspar.

Appendix 2, Pyroxene analyses continued

sample	type	SiO_2	Al_2O_3	TiO_2	FeO^t	MnO	MgO	CaO	Na_2O	K_2O	P_2O_5	Cr_2O_3	Sum	Ca	Mg	Fe
19359T	ass	48.46	.42	.34	30.30	1.30	.47	18.19	.55	0	0	.02	100.04	42.8	1.5	55.7
		48.33	.43	.35	29.57	1.19	.81	19.25	.43	0	0	.01	100.37	44.3	2.6	53.1
		48.10	.42	.34	29.80	1.16	.80	19.24	.43	0	0	.01	100.30	44.1	2.6	53.3
	l	52.09	3.33	1.49	7.75	.18	15.19	20.77	.32	0	0	.17	101.29	43.3	44	12.6
19337		48.06	.36	.32	30.43	1.16	.53	18.88	.46	0	.01	0	100.22	43.5	1.7	54.8
		47.99	.41	.43	29.44	1.20	.77	18.91	.42	.01	0	.01	99.61	44	2.5	53.5
		47.89	.35	.38	29.70	1.26	.59	19.04	.46	0	0	0	99.68	44.2	1.9	53.8
		48.69	.36	.35	30.61	1.21	.55	19.16	.50	.01	0	0	101.45	43.7	1.8	54.5
		48.27	.46	.39	30.44	1.23	.84	19.95	.43	0	0	.01	102.02	44.5	2.6	53
		47.92	.36	.35	30.37	1.15	.46	19.38	.46	0	.01	.01	100.46	44.3	1.5	54.2
		47.58	.36	.31	30.04	1.17	.60	18.76	.45	.01	.01	0	99.28	43.6	1.9	54.5
		47.71	.39	.42	30.31	1.23	.43	18.86	.48	0	0	.09	99.93	43.7	1.4	54.9
30483	c	47.65	.37	.34	30.18	1.26	.52	19.54	.46	0	0	.01	100.33	44.6	1.6	53.8
	c	47.78	.46	.36	29.94	1.10	.96	19.61	.45	0	0	0	100.66	44.2	3	52.7
	i	47.73	.41	.29	29.62	1.12	.71	19.44	.41	0	0	0	99.72	44.6	2.3	53.1
	r	47.77	.38	.34	29.68	1.23	.63	19.14	.50	0	.01	.04	99.71	44.3	2	53.6
	r	47.11	.34	.30	30.35	1.22	.50	19.48	.46	0	0	.02	99.78	44.4	1.6	54
	c	47.76	.44	.43	30.69	1.26	.52	19.56	.44	0	.02	0	101.12	44.2	1.6	54.2
	r	47.86	.34	.40	30.53	1.13	.30	19.41	.55	0	0	.03	100.54	44.5	.9	54.6
	c	47.82	.39	.33	30.16	1.29	.69	19.88	.47	0	0	0	101.01	44.8	2.1	53.1
	r	48.18	.27	.30	30.60	1.24	.26	19.61	.57	.02	.05	0	101.11	44.7	.8	54.5
	rlc	48.53	1.13	.90	23.79	.90	4.99	20.01	.30	0	0	.02	100.58	44	15.3	40.8
	rlr	49.28	.95	.69	20.97	.80	6.85	20.26	.33	0	.01	.04	100.19	43.9	20.7	35.5
19420		46.10	.37	.43	31.85	1.09	.47	18.58	.52	0	0	0	99.40	42.1	1.5	56.4
		48.16	.43	.45	31.22	1.06	.99	18.72	.50	0	0	0	101.53	42.1	3.1	54.8

Appendix 2, Pyroxene analyses continued

sample	type	SiO_2	Al_2O_3	TiO_2	FeO^t	MnO	MgO	CaO	Na_2O	K_2O	P_2O_5	Cr_2O_3	Sum	Ca	Mg	Fe
19420		43.39	.78	.92	30.84	1.01	.33	17.71	1.02	.09	0	0	96.09	41.9	1.1	57
		43.88	.71	1.17	81.12	1.12	.32	17.61	.94	.05	0	0	96.91	41.6	1.1	57.4
		45.16	.31	.41	32.46	1.12	.40	18.65	.48	0	.03	.02	99.04	41.9	1.3	56.9
		45.88	.40	.44	32.50	1.13	.41	18.65	.52	0	0	0	99.93	41.8	1.3	56.9
		48.07	.31	.32	30.60	1.23	.32	18.98	.52	.04	.01	.02	100.44	43.8	1	55.1
		48.47	.32	.33	32.12	1.20	.31	19.20	.48	.02	0	.04	102.49	43	1	56.1
		48.52	.36	.36	30.13	1.25	.53	19.71	.45	0	0	.04	101.36	44.8	1.7	53.5
		47.96	.41	.36	30.87	1.33	.37	19.04	.45	.07	0	.02	100.89	43.6	1.2	55.2
		44.59	.24	.40	31.31	1.19	.29	18.51	.54	.01	0	0	97.09	42.7	.9	56.4
		45.01	.34	.32	30.42	1.25	.52	18.61	.47	0	.03	0	96.97	43.2	1.7	55.1
		46.89	.27	.36	30.39	1.23	.35	18.67	.53	.05	0	0	98.75	43.6	1.1	55.3
22154	c	46.52	.26	.37	30.44	1.28	.35	18.87	.52	.02	.03	0	98.65	43.8	1.1	55.1
	r	45.46	.25	.27	30.49	1.17	.30	18.70	.52	0	.03	.01	97.20	43.6	1	55.5
	c	46.44	.50	.39	30.36	1.29	.96	19.23	.43	0	.03	0	99.64	43.4	3	53.5
	c	46.13	.39	.33	29.99	1.19	.46	18.25	.50	0	.01	.02	97.29	43.1	1.5	55.3
	r	46.56	.29	.31	30.92	1.17	.33	18.14	.52	0	0	.01	98.25	42.5	1.1	56.5
	c	50.82	.51	.06	17.53	1.20	8.76	20.99	.39	0	.04	0	100.29	44.8	26	29.2
	c	48.05	.34	.21	18.23	1.24	7.87	21.03	.40	.01	0	.01	97.38	45.5	23.7	30.8
	c	48.36	.51	.32	23.59	1.07	4.75	20.28	.40	0	0	0	99.28	44.8	14.6	40.7
	c	48.92	.48	.15	17.86	1.37	8.21	20.62	.38	0	0	.02	98.01	44.8	24.8	30.3
	c	49.13	.44	.29	22.63	1.22	5.64	19.27	.44	0	.07	0	99.12	43	17.5	39.5
	c	48.62	.41	.16	22.76	1.12	5.37	19.58	.42	.04	.02	0	98.50	43.7	16.7	39.6
	i	47.23	.32	.44	30.67	1.26	.40	19.37	.46	0	.07	.04	100.26	44.2	1.3	54.6
	r	46.99	.50	.37	29.51	1.15	.52	18.28	1.22	.06	.01	.02	98.65	43.5	1.7	54.8
30476	c	47.15	.31	.45	30.70	1.14	.32	19.12	.50	.01	0	.01	99.71	43.9	1	55.1
	r	47.69	.26	.36	30.31	1.13	.29	19.02	.52	.01	.02	0	99.61	44.1	.9	54.9

Appendix 2, Pyroxene analyses continued

sample	type	SiO_2	Al_2O_3	TiO_2	FeO	MnO	MgO	CaO	Na_2O	K_2O	P_2O_5	Cr_2O_3	Sum	Ca	Mg	Fe
19342		48.27	.49	.55	29.31	1.27	.98	18.78	.44	0	0	0	100.09	43.7	3.2	53.2
		47.56	.47	.40	30.00	1.34	1.14	19.63	.44	0	.02	0	101.00	44.	3.6	52.5
	rd	45.89	.36	.38	31.04	1.25	.13	18.31	.47	.05	.01	0	97.88	42.9	.4	56.7
	mh	46.61	.98	1.22	30.09	1.29	.42	18.52	.48	.05	.01	.02	99.70	43.5	1.4	55.1
	mh	45.06	.58	1.06	30.41	1.39	.34	18.34	.47	.09	0	0	97.74	43.1	1.1	55.8
	mh	43.77	.75	1.19	29.96	2.41	.38	18.56	.54	.04	0	0	97.60	43.7	1.2	55.1
	mh	42.36	.94	.99	30.05	1.23	.45	18.52	.48	.04	.05	0	95.10	43.5	1.5	55.1
	mh	44.37	.77	.87	29.60	1.26	.45	18.23	.44	.05	.02	0	96.07	43.5	1.5	55.1
	q	46.92	.83	.68	32.16	1.64	.48	16.14	.41	.04	.03	.06	99.39	38.5	1.6	59.9
	q	47.23	.78	.37	30.55	1.80	.50	17.22	.42	.05	.01	0	98.93	41.2	1.7	57.1
30474		48.26	.29	.43	30.31	1.17	.37	19.08	.53	.01	0	0	100.46	44.1	1.2	54.7
		48.92	.34	.37	30.27	1.22	.54	18.37	.53	.05	0	0	100.60	43	1.8	55.3
		47.71	.40	.34	30.52	1.32	.49	18.44	.53	0	.01	.01	99.79	42.9	1.6	55.5
22042		48.85	.41	.60	30.59	1.50	.24	18.46	.50	.05	.03	0	101.22	43.3	.8	56
		49.38	.51	.40	29.52	1.22	1.34	19.47	.44	.02	0	0	102.31	43.9	4.2	51.9
		49.07	.51	.33	29.36	1.20	1.44	19.88	.46	.01	.01	.01	102.29	44.4	4.5	51.1
		47.95	.29	.28	30.92	1.26	.43	20.05	.46	0	0	.03	101.67	44.8	1.3	53.9
		47.6	.29	.38	30.93	1.18	.33	19.86	.46	.04	0	0	101.07	44.7	1	54.3

Type explanation: c, core. r, rim. i, intermediary postion. l, light pyroxene. ass, pyroxene associated with the zonar pyroxene above in aggregate. rlc, rlr, light resorbed pyroxene in acid glass, core and rim respectively. rd, pyroxene rod. mh, microphenocryst in hybrid fiamme. q, quench pyroxene in acid quench clot.

Appendix 3, Olivine analyses

Sample	type	SiO_2	Al_2O_3	TiO_2	FeO^t	MnO	MgO	CaO	Na_2O	K_2O	P_2O_5	Cr_2O_3	Sum	Fo	Fa
19359T		30.95	.0	.03	69.58	2.74	.18	.35	0	.03	.01	0	103.86	.5	99.5
		29.88	0	.06	68.26	3.10	.14	0	.04	0	0	.01	101.49	.4	99.6
		30.03	0	0	67.53	2.96	.15	0	.03	0	0	0	100.70	.4	99.6
		30.25	0	.04	68.73	3.24	.20	0	0	0	0	0	102.44	.5	99.5
		29.80	.01	0	67.71	3.01	.17	0	0	0	0	0	100.70	.5	99.5
19337		31.41	0	.03	68.10	3.07	.16	.37	.06	.01	0	.01	103.22	.4	99.6
		30.28	.01	.05	67.41	3.01	.16	.39	.03	.02	0	0	101.36	.4	99.6
		30.91	.02	.11	67.66	2.96	.16	.33	.06	.04	0	.01	101.36	.4	99.6
		29.79	.01	.06	69.36	2.96	.16	.34				.04	102.94[x]	.4	99.6
19420		31.04	.03	.47	69.22	3.03	.20	.38	.03	0	.01	.01	104.41	.5	99.5
		30.77	.03	0	69.51	3.28	.18	.35	.04	0	0	0	104.17	.5	99.5
		30.51	0	.05	69.55	2.95	.19	.33	.06	0	.02	0	103.66	.5	99.5
19342		30.86	0	.10	66.69	3.53	.15	.37	.03	.02	.01	.06	101.82	.4	99.6

x: sum includes ZnO:.23

Appendix 4, Ilmenite analyses

sample	SiO_2	Al_2O_3	TiO_2	FeO^t	MnO	MgO	CaO	Cr_2O_3	V_2O_3	NiO	ZnO	Sum	Ilm	Hæm
19337	.02	.02	48.19	48.60	1.42	.02	0	0	-	-	-	98.32	92.6	7.4
	.10	.01	47.38	48.38	1.43	0	.01	0	-	-	-	97.30	92.1	7.9
	0	0	46.97	47.87	1.45	.03	0	0	-	-	-	96.31	91.9	8.1
	.10	.03	48.94	48.14	2.03	.05	0	.02	.17	.01	.01	99.50	93	7
	.06	.01	49.51	48.12	2.34	.02	.01	0	.15	.02	.08	100.32	93.2	6.8
	.06	.01	49.30	48.59	1.50	.03	0	0	.12	0	.13	99.74	93.5	6.5
	.01	.02	48.62	49.65	1.41	.04	0	.01	.15	.08	.11	100.23	91.4	8.6
	.06	0	48.88	48.48	1.53	.04	0	0	.15	0	.24	99.38	92.9	7.1
	.05	.03	51.10	50.66	1.46	.01	.08	0	.16	.04	.09	103.68	93.2	6.8
	.14	.01	48.24	50.08	1.42	0	.61	.01	.18	.08	0	100.77	90.3	9.7
19420	.10	.04	47.70	48.10	1.44	.04	.35	0	-	-	-	98.68	92.1	7.9
	.08	.02	50.66	49.26	1.61	.04	0	.01	-	-	-	101.69	94.3	5.7
	.08	.01	49.53	48.97	1.64	.01	.02	.04	-	-	-	100.29	93.4	6.6
19359T	.12	.01	47.71	49.10	1.42	.04	.05	.32	-	-	-	98.77	91.6	8.4
	.01	.04	48.97	49.97	1.16	.03	.06	.02	-	-	-	100.26	92.2	7.8
	.10	.02	48.13	18.80	1.16	.04	0	0	-	-	-	98.23	92.7	7.3
	.08	.03	49.60	49.14	1.34	.03	.03	0	-	-	-	100.25	93.6	6.4
	.05	.02	48.30	48.41	1.37	.01	.04	0	-	-	-	98.20	93.	7.
	.02	.02	48.04	48.03	1.30	.03	.07	0	-	-	-	97.51	93.	7.
	.03	.02	48.57	49.00	1.24	.02	.04	0	-	-	-	98.93	92.8	7.2
19342 sc	.06	.02	50.06	49.10	1.74	.01	0	.02	-	-	-	101.01	93.7	6.3
sr	.03	.03	46.58	51.03	1.74	.02	.02	.02	-	-	-	99.60	88.	12.
mh	.16	0	46.81	46.50	1.99	.02	.02	0	-	-	-	95.50	92.7	7.3
22154 zp	.03	.02	48.70	48.11	1.47	.02	.02	.03	-	-	-	98.40	93.5	6.5
30476	.04	.03	47.22	47.38	1.31	.02	.10	0	-	-	-	96.10	92.8	7.2
22042	.07	.05	46.47	48.46	1.38	.04	.08	0	-	-	-	96.55	90.8	9.2
	.04	.03	51.75	46.57	1.29	.01	0	0	-	-	-	99.69	98.6	1.4

Type explanation: sc,sr, core and rim from sceletal phenocryst. mh, microphenocryst from hybrid fiamme. zp, from zonar pyroxene group.

Appendix 5, Magnetite analyses

sample	type	SiO_2	Al_2O_3	TiO_2	FeO^t	MnO	MgO	CaO	Na_2O	K_2O	Cr_2O_3	Sum	Usp	Mgt
19337	-	.28	.44	22.11	70.40	1.15	.03	.53	-	-	0	94.93	65.8	34.2
19420	-	.17	.31	20.61	70.81	1.18	.01	.33	-	-	0	93.42	61.8	38.2
19359T	-	1.17	.39	19.00	74.11	.81	0	.23	-	-	.06	95.93	61.5	38.5
	agg	.14	.39	18.87	71.75	1.07	.09	0	-	-	.01	92.36	59.5	40.5
	agg	.12	.34	19.36	72.49	1.11	.01	0	-	-	.04	93.50	60.2	39.8
	agg	.20	.35	20.23	72.58	.95	.02	0	-	-	.03	94.42	62.2	37.8
19342	q[a]	14.65	4.32	14.11	56.07	.74	.04	.74	1.25	.54	.01	96.41	-	-
	q[b]	.42	0	19.72	78.24	1.03	.04	.59	-	-	.01	100.05	57.5	42.5
22154	zpx	.18	.36	18.53	75.74	1.00	.02	.05	-	-	.01	95.89	56.	44.
	zig	1.31	.37	27.83	65.42	1.05	.03	.08	-	-	.05	94.14	84.6	15.4
	zf	.19	.02	17.08	76.74	.98	.02	0	-	-	0	95.03	52.	48.
	-	.20	.54	21.22	72.26	1.08	0	.12	-	-	0	95.42	65.	35.
	-	.09	.39	21.27	68.16	1.14	.04	.04	-	-	0	91.13	67.5	32.5
30474	-	.13	.39	20.22	73.26	.10	.02	.38	-	-	.01	95.41	60.	40.
22042	-	.38	.47	21.42	69.67	1.11	.05	.07	-	-	.03	93.20	68.1	31.9
	-	.59	.48	22.20	70.04	1.04	.05	.09	-	-	0	94.49	70.2	29.8
	-	.29	.40	22.92	66.01	1.02	.01	.28	-	-	0	90.93	74.	26.

a) original analysis, b) recalculated to 100 after subtraction of 22% anorthoclase.

Type explanation: agg, from aggregate of pyroxene, feldspar and magnetite. q, acicular magnetite from acid quench clot. zpx, in zonar pyroxene. zig, in glass inclusion in zonar pyroxene. zf, from inclusion in feldspar in zonar pyroxene group.

Appendix 6, Chevkinite partial analyses

sample	type	SiO_2	Al_2O_3	TiO_2	FeO^t	MnO	MgO	CaO	Na_2O	K_2O	P_2O_5	Sum
19337	-	18.91	.24	18.09	12.40	0	.01	3.39	.08	.04	.05	53.20
	-	18.22	.25	18.94	12.16	0	.02	3.65	0	.03	0	53.26
19359T	-	19.14	.22	20.83	11.80	0	.02	3.91	0	0	.08	56.00
	-	18.77	.24	20.10	12.19	0	0	3.60	0	.02	.01	54.92
19420	-	17.21	.24	19.99	12.26	0	0	3.30	0	.05	.04	53.08
	-	16.84	.25	19.75	12.39	0	0	3.29	0	.07	.06	52.65
	-	18.80	.21	20.54	12.09	0	0	3.90	0	.04	.04	55.63
	-	18.11	.21	20.04	11.70	0	.03	3.92	0	.04	.02	54.08
19342	-	17.83	.26	20.15	11.84	0	.01	3.54	0	0	.03	53.17
	-	17.26	.25	20.12	11.78	.01	0	3.81	0	.02	.07	53.32
	-	17.03	.26	-	11.42	-	0	3.86	0	.01	-	32.67[x]
22042	-	18.56	.27	18.86	11.81	0	.02	3.61	0	.05	.08	53.25

x: includes BaO:.04, SrO:.04

Appendix 7, Mafic groundmass phases from sample 19337

sample	type	SiO_2	Al_2O_3	TiO_2	FeO[T]	MnO	MgO	CaO	Na_2O	K_2O	P_2O_5	Sum	Ca	Mg	Fe
19337	arf	50.07	.74	-	35.07	-	-	1.34	6.18	.61	-	93.10			
	arf	51.95	1.15	.63	39.25	2.23	.09	.60	5.91	.85	0	102.66			
	arf	46.95	2.74	.80	37.32	2.07	.05	.54	5.79	1.38	0	97.63			
	æn	40.65	.39	6.91	45.90	1.03	.10	.28	7.08	.03	0	102.36			
	æn	40.26	.41	7.25	45.26	.96	.06	.30	6.96	.01	.05	101.52			
	px	46.54	.27	.51	30.93	1.23	.12	18.79	.56	0	0	98.96	43.6	.4	56
	px	46.98	.28	0	30.65	1.17	.14	18.51	.48	.02	.01	98.30	43.4	.5	56.1
	ol	30.36	.03	.06	66.94	3.06	0	.01	.05	.03	.01	100.54			
	ol	29.65	0	.10	67.16	3.07	0	0	.04	0	.02	100.05			

Type explanation: arf, arfvedsonite. æn, ænigmatite. px, pyroxene. ol, olivine.

Appendix 8, Acid glass analyses

sample	type	SiO_2	Al_2O_3	TiO_2	FeO^t	MnO	MgO	CaO	Na_2O	K_2O	P_2O_5	Sum
19337	I	76.01	11.96	.16	2.89	.06	0	.36	4.60	5.18	0	101.22
	I	74.83	11.85	.18	2.73	.05	.03	.36	4.60	5.23	0	99.86
	I	76.00	11.74	.23	2.87	.08	.02	.29	4.60	5.31	.02	101.16
	I	76.00	11.54	.17	2.79	.06	.02	.29	4.44	5.40	.01	100.72
	I	75.80	11.82	.17	2.77	.06	.03	.31	4.58	5.27	0	100.81
	II	76.30	11.45	.14	3.20	.08	.02	.31	4.40	4.35	.03	100.28
	III	73.15	11.75	.18	2.77	.06	.02	.32	4.25	5.21	.01	97.72
	II	76.49	11.67	.21	2.83	.08	.02	.35	4.48	5.31	0	101.44
	III	74.03	11.67	.15	2.92	.07	0	.36	4.41	5.25	.02	98.88
	V	73.67	11.07	.15	2.72	.05	.08	.24	5.57	2.53	.02	96.10
	VI	75.32	11.72	.18	2.78	.12	.02	.31	4.41	4.96	.02	99.84
	VI	75.37	11.64	.17	2.91	.04	0	.38	4.51	4.67	.01	99.70
	VI	75.80	11.53	.16	2.96	.05	.02	.28	4.55	4.97	.01	100.33
	VII	75.06	11.68	.19	2.83	.04	.02	.34	4.73	4.76	.01	99.66
	VII	73.97	11.67	.17	2.81	.08	.02	.45	4.29	4.78	0	98.24
30483	s	74.12	11.12	-	2.57	-	-	.19	4.61	3.78	-	96.39
	s	76.76	11.71	-	3.03	-	-	.35	5.03	4.10	-	100.98
	s	73.50	11.95	-	2.60	-	-	.35	5.31	4.02	-	97.73
	s	72.04	11.67	-	3.05	-	-	.44	5.00	4.32	-	96.51
	s	75.56	11.88	-	2.50	-	-	.35	4.76	4.04	-	99.08
	s	77.65	11.87	-	2.87	-	-	.31	5.14	4.21	-	102.05
	p	73.47	11.45	-	2.48	-	-	.38	4.70	3.80	-	96.28
	p	70.73	11.20	-	2.32	-	-	.41	4.85	3.82	-	93.36
	p	73.59	11.40	-	2.41	-	-	.37	4.61	3.86	-	96.23
	p	74.68	12.60	-	2.35	-	-	.42	3.69	5.05	-	98.79
	p	73.70	11.90	-	2.90	-	-	.28	5.18	4.53	-	98.49
	obs	75.10	12.01	-	2.53	-	-	.44	5.02	4.16	-	100.16
	obs	74.31	11.82	-	2.66	-	-	.27	5.09	4.26	-	98.41
	obs	74.02	11.93	.01	3.05	.06	0	.42	4.91	4.30	.01	98.71
	l	70.08	12.65	-	4.09	-	-	1.25	4.52	4.53	-	97.12
	l	68.49	12.88	-	4.17	-	-	1.18	4.02	4.17	-	94.92
	l	69.00	12.77	.43	4.55	.12	.15	1.27	4.16	4.47	0	96.92
19420	f	69.57	10.87	.14	2.41	.09	.01	.41	4.74	4.15	0	92.39
	f	69.08	10.98	.15	2.56	.05	.02	.44	4.66	4.18	.03	92.15
	f	69.58	11.05	.20	2.53	.09	.01	.31	4.78	4.27	.02	93.29
	s	71.98	11.29	.18	2.85	.07	.04	.38	4.83	4.34	.01	95.97
	s	70.61	11.23	.19	2.73	.04	.01	.34	4.73	4.23	.01	94.12
	s	74.45	10.93	.16	2.94	.06	.01	.37	4.59	4.27	.01	97.76
	s	74.40	10.85	.18	2.92	.06	.01	.34	4.74	4.32	.01	97.83
	s	72.64	11.14	.17	2.87	.10	.01	.36	4.83	4.29	.01	96.42
19416	s	74.36	11.59	.15	2.55	.07	.03	.39	4.85	4.10	.01	98.10
	l	71.03	13.14	.26	3.25	.17	.05	1.20	5.31	3.54	.03	97.98
19342	fh	68.46	13.07	.16	3.22	.17	.02	.43	4.84	4.50	.01	94.88
	fh	66.69	11.60	.43	2.90	.10	.01	.34	4.53	4.24	.04	90.88
	fh	67.77	11.06	.09	2.29	.07	.08	.38	3.83	4.21	.04	89.82
	fh	70.19	11.33	.22	2.12	.06	.04	.39	4.23	4.25	.08	92.91

Appendix 8, Acid glass analyses continued

sample	type	SiO_2	Al_2O_3	TiO_2	FeO^t	MnO	MgO	CaO	Na_2O	K_2O	P_2O_5	Sum
30476	p	70.22	11.55	.31	2.52	.12	0	.38	4.67	4.09	.04	93.90
	p	71.86	11.46	.07	2.84	.10	0	.36	4.72	4.01	.02	95.44
	mc	71.67	8.82	.11	1.31	0	.34	.54	3.19	3.58	.16	89.72
	s	73.03	11.58	.16	2.86	.17	.02	.33	4.74	3.91	.02	96.52
	s	74.32	11.50	.16	2.79	.02	0	.37	4.87	4.22	0	98.25
	s	72.97	11.49	.32	2.93	.06	0	.41	3.74	4.16	.01	96.09
30474	s	73.37	11.37	.18	2.91	.07	0	.40	4.89	4.21	.01	97.41
	s	73.59	11.18	.16	2.84	.08	.02	.43	4.89	4.26	.01	97.34
	s	69.79	10.73	.13	2.55	.06	.01	.43	4.60	4.02	.02	92.34
	l	69.27	13.26	.39	4.80	.19	.13	1.33	5.37	3.77	.03	98.54
22042	s	75.68	11.23	.19	2.76	.07	.01	.42	4.86	4.13	.01	99.35
	s	73.64	10.96	.21	2.69	.05	0	.43	4.78	4.12	0	96.88
	s	74.09	11.98	.11	2.54	.06	0	.40	5.15	3.99	.05	98.37
	s	74.14	11.87	.06	2.45	.09	0	.49	5.01	3.57	0	97.68
	s	71.98	10.91	.23	2.57	.09	.06	.42	4.76	3.43	0	94.45

Type explanation: roman numerals, fields of analysis in sample 19337. s, shard analysis. p, pumice analysis. obs, little vesiculated obsidian fragment. l, low silica shard or pumice fragment. f, fiamme in welded vitric ignimbrite. fh, hybrid fiamme. mc, microcrystalline fragment.

Appendix 8, Acid glass analyses (OH programme)

sample	type	SiO_2	Al_2O_3	TiO_2	FeO^t	MnO	MgO	CaO	Na_2O	K_2O	F	Cl	Sum
19337	VIII	76.84	11.39	.26	2.85	.16	0	.28	4.43	5.18	0	.27	101.60
	VIII	74.56	11.32	.27	2.41	.07	.03	.35	4.59	5.26	0	.28	99.08
	VIII	77.76	11.44	.15	2.27	.09	0	.37	4.53	5.38	.38	.22	102.38
	IX	74.71	11.37	.10	2.73	.03	.03	.39	4.66	5.12	.07	.22	99.35
	IX	72.02	11.67	.16	2.32	.13	.01	.42	4.61	5.09	.24	.29	96.79
	IX	75.18	11.59	.23	2.10	.06	0	.29	4.65	5.55	.24	.27	100.00
	IX	72.64	11.60	.17	1.97	.02	0	.36	4.55	5.24	.10	.26	96.81
	IX	75.67	11.41	.08	2.26	.07	0	.38	4.48	5.44	.12	.30	100.09
22042	s	72.01	11.26	.06	2.48	.08	0	.43	4.77	3.99	0	.26	95.28
	s	72.87	11.54	.15	2.89	.05	.02	.41	4.91	4.05	.05	.29	97.14
	s	72.12	11.54	.25	2.44	.04	.01	.38	4.97	4.01	0	.26	95.96
	s	73.84	11.79	.07	2.72	0	0	.42	4.97	4.03	0	.29	98.06
	s	75.51	11.75	.08	3.02	.03	.01	.49	5.13	4.19	.05	.28	100.46
	s	71.06	11.67	.24	2.58	.04	.02	.34	5.17	4.08	.02	.33	95.47
	p	69.82	11.43	.12	3.54	.05	.14	.36	4.44	2.97	0	.18	93.01
	p	69.56	12.17	.18	4.00	.07	.01	.99	5.12	3.93	.05	.15	96.18
	het	73.51	13.03	.11	3.05	.09	.01	.64	5.37	3.31	0	.20	99.27

Sum corrected for F and Cl

explanation: roman numerals; fields in sample 19337. s, shard. p, pumice. het, heterogeneous looking clast.